nature ecology & evolution

Article

https://doi.org/10.1038/s41559-022-01910-z

Evidence for the cooking of fish 780,000 years ago at Gesher Benot Ya'aqov, Israel

In the format provided by the authors and unedited

Supplementary Materials for

EVIDENCE FOR THE COOKING OF FISH 780,000 YEARS AGO AT GESHER BENOT YA'AQOV, ISRAEL

Irit Zohar[1,2*], Nira Alperson-Afil[3], Naama Goren-Inbar[4], Marion Prévost[4], Thomas Tütken[5], Guy Sisma-Ventura[6], Israel Hershkovitz[7#], and Jens Najorka[8#]

Supplementary Text: Materials, Methods, and Results

Supplementary Text A-F:

A. THE GBY SITE

Archaeological sites of early hominids in the vicinity of freshwater lakes have been observed in Africa since the Early Pleistocene, ca. 1.95 Ma[1-5]. The dispersal route out of Africa, along the Rift Valley, is also associated with freshwater habitats, as evidenced in the location of 'Ubeidiya (1.5 Ma; three km south of present-day Lake Kinneret)[4,6-8] and Gesher Benot Ya'aqov (GBY; 0.78 Mya) (Extended Data Fig. 1a)[9].

Gesher Benot Ya'akov (GBY) is a waterlogged site located on the shores of paleo-Lake Hula in the northern Jordan Valley, Israel (Extended Data Fig. 1)[9,10]. The archaeological site is embedded in the Benot Ya'akov Formation (characterized by the endemic fossil gastropod *Viviparus apameae*). The stratigraphic units at GBY were characterized according to a 34 m thick sequence of fine-grained tectonically tilted layers, with organic-rich and carbonate-rich muds of autochthonous origin (gravelly or molluscan sand; fine-grained offshore mud; mollusk coquina)[11,12]. These represent different depositional lake margin/beach environments, documenting an oscillating freshwater lake assigned to the Early to Middle Pleistocene (MIS 18–20[9-14]). The archaeological material, deposited during periods of a drop in lake level, represents a defined and distinct cultural entity, identified as an archaeological horizon (AH)[9].

Three main areas were excavated: A, B, and C (Extended Data Fig. 1c), revealing more than 15 AHs (separated by layers and levels) and yielding rich lithic, botanical, and faunal assemblages[9,15-28]. Area A (AHs: I-4 and I-5) was excavated only during the first season[9]. It was poor in lithic artifacts compared with Area B, but rich in fish remains[27], crabs[29], and birds[9]. Area B constituted a main focus of the GBY excavations, as it contained the highest number of AHs, displaying four Layers (II-2/3, II-5, II-5/6, II-6). An exceptional sequence of eight superimposed AHs (each with a thickness of 10–20 cm) was exposed at Layer II-6 (levels: L1, L2, L3, L4, L4b, L5, L6, L7)[11,12]. The AHs of II-6 L1–7 provided an immense archive of the Acheulian culture, with rich lithic artifacts made of flint, basalt, and limestone, including typical Acheulian hand-axes and cleavers[9]. The vertebrate remains, studied from various AHs in areas B, and C, comprised large (*Hippopotamus amphibius*, *Palaeoloxodon antiquus*), medium (*Dama* sp.), and micro-

vertebrates (micro-mammals, reptiles, and amphibians (Supplementary Table 1)[9,20,21,30,31]. The macro-botanical remains were well preserved and comprised wood and bark[32], as well as 55 taxa of nuts, fruits, seeds, and vegetables, attesting to a varied plant diet[28]. The exceptional abundance of cultural material, as well as faunal and botanical remains, emphasizes that extensive activities of hunting, gathering, fishing and processing were carried out by large groups of hominins all year round[28,33,34].

Supplementary Table 1. Terrestrial vertebrate remains (by size group) identified at GBY (total number of identified specimens (NISP), frequency, and taxon richness (S')), according to excavated areas (B, C) and archaeological horizons (data after[30]). The sequential AHs of II-6: L1 to L7 are marked in light blue.

		Vertebrate NISP				
Excavated Area	**AH**	**Medium-large mammals**	**Micro-vertebrates**	**Total**	**Frequency**	**S'- Large mammals**
B	II-2	37	446	483	9.06	6
	II-2/3	29	154	183	3.43	4
	II-5	28	119	147	2.76	3
	II-5/6	4	3	7	0.13	4
	II-6 L1	66	206	272	5.10	7
	II-6 L2	14	35	49	0.92	4
	II-6 L3	14	63	77	1.44	3
	II-6 L4	45	82	127	2.38	8
	II-6 L5	24	33	57	1.07	5
	II-6 L6	29	52	81	1.52	9
	II-6 L7	219	737	956	17.93	14
C	V-5	754	100	854	16.01	14
	V-6	1,400	640	2,040	38.25	14

In GBY II-6 L1–7 large numbers of burnt flint microartifacts were recovered and thoroughly studied, integrating paleoenvironmental data, including various factors involved in the complex process of fire ignition, combustion, and early hominin behavior in respect to controlled fire. The results of these studies indicate that natural, recurrent, fires were not the cause of the anthropogenic material burning observed at GBY. Rather, there is clear evidence of fire monitoring by the hominids on site[9,16,26,35-39]. Furthermore, the comprehensive spatial analyses of burnt flint microartifacts demonstrated the use of fire throughout the long stratigraphic sequence at GBY, suggesting that it was a continuous practice of the Acheulian hominids. The hominids occupying GBY likely possessed the ability to produce fire at will and had a deep knowledge of maintaining and using fire [35,37,39].

GBY Fish Remains

Fish remains were abundant at all excavated AHs, with Area A (natural death) revealing the presence of three out of the five native families documented from Lake Hula[27,40]: Cichlidae (tilapiini), Clariidae (catfish), and Cyprinidae (carps). In the eight sequentially superimposed AHs of Area B (II-6: L1–7; Fig. 1; Supplementary Table 2), we observed a unique pattern of preservation: a wealth of cyprinid pharyngeal teeth (fifth ceratobranchial; Extended Data Fig. 2) and a near absence of fish bones. These eight AHs are the focus of the present study, as they provide evidence of a continuous behavioral pattern involving an association of fish remains with rich anthropological assemblages (Extended Data Fig. 1d).

Supplementary Table 2. The total number of fish remains (NISP) recovered at GBY, and the rates (%) of taxonomic identification to family level, by excavated areas (A, B, C) and archaeological horizons (AHs)[9,11]. In the eight sequential AHs recovered at Area B (II-6 L1–7; marked in light blue), the low rates of unidentified fish demonstrate the high level of success in taxonomic identification.

GBY Excavated Area	AH	Sediment	NISP*	% Cichlidae	% Clariidae	% Cyprinidae	% Unid.
A	I-4	Black mud	6,014	6.00	2.00	92.00	0.00
	I-5	Coquina	3,192	2.50	0.50	97.00	0.00
B	II-2	Coquina	1,049	4.00	0.40	93.00	2.30
	II-2/3	Coquina/ Black mud	1,590	6.50	1.00	68.00	24.50
	II-5	Black mud	1,442	5.10	0.90	81.00	13.00
	II-6 L1	Black mud	2,644	0.00	0.00	100.00	0.00
	II-6 L2	Black mud	2,612	0.80	0.04	99.16	0.00
	II-6 L3	Grey mud	5,060	0.02	0.02	99.96	0.00
	II-6 L4	Grey mud	4,827	0.08	0.00	99.92	0.00
	II-6 L4b	Coquina	679	0.00	0.00	100.00	0.00
	II-6 L5	Coquina	2,741	0.00	0.00	100.00	0.00
	II-6 L6	Coquina	1,921	0.10	0.00	99.90	0.00
	II-6 L7	Coquina	5,753	0.90	0.40	98.70	0.00
C	V-3	Coquina	36	3.00	0	97.00	0
	V-4	Sand	40	2.50	0	92.50	5.00
	V-4/5	Sand/ Coquina	73	1.30	0	96.0	2.70
	V-5	Coquina	2,445	1.50	0.08	98.00	0.42
	V-6	Black mud	1,416	2.00	73.00	20.00	0

* NISP (= no. of identified specimens) comprising complete and fragmented bones and teeth.

B. CYPRINIDAE

Cyprinidae (carp) constitute one of the most widespread and diverse (> 1,200 extant species) families in freshwater habitats[41-44]. Being primary freshwater fish, Cyprinidae distribution patterns and speciation closely reflects the geological evolution of the landscape[45,46]. Previous to its drainage, in the early 1950s, eight species of cyprinids existed in the lake, with body size ranging from 10 to 80 cm in total length (TL)[40,44,47,48]. Among them were the now extinct species *Mirogrex hulensis,* once endemic to Lake Hula, and the extant *Luciobarbus longiceps* (Jordan barbel; Valenciennes 1842) which is endemic to the Jordan River basin[40,44,47-49]. The members of this family typically have one or more pairs of barbels (fleshy protuberances) near the mouth (Extended Data Fig. 2a), used to search for food, and often possess large, shiny scales.

From a nutritional perspective, fish have a high nutritional value, containing 19% protein, 8% fat, 0.5% calcium, 0.25% phosphorus and 0.1% vitamins A, D, B, C. They are also an important source of the n-3 highly unsaturated fatty acids (HUFA), eicosapentaenoic (EPA) and docosahexaenoic (DHA)[50-52]. It has been recorded that in artisanal fishing communities, fat fish, such as carp, is regarded as a preferred food for children, since they supply unique long-chain fatty acids and essential micronutrients that influence growth, cognitive development, and overall health[53]. Fishery data from Lake Hula (1951-1958) show that large species of cyprinids were considered as an important food source, and that a decrease in water level was associated with an increase in *L. longiceps* fishery[49].

From an osteological perspective, fish belonging to the family Cyprinidae are characterized by a lack of teeth in their oral jaws and the appearance of well-developed teeth on the pharyngeal jaws (fifth ceratobranchials; Extended Data Fig. 2)[54-56]. The number of pharyngeal teeth on each bone (4–15), their structure and arrangement on the bone (1–3 rows)[57], reflect morphological adaptations associated with diet and have been used as criteria for classification to species level[27,41,55,58-61]. Since oral and pharyngeal teeth are homologous[62], they share a similar tooth structure: a central dental mesenchyme surrounded by an

external mineralized layer (enameloid and dentin). The tooth connects to the pharyngeal bones via the "bone of attachment", a shaft of mineralized tissue[63-65].

Cyprinids, like other tooth-bearing teleosts, display a continuous and lifelong tooth formation and replacement process in each row[66,67]. Each row replaces its teeth independently, and each species replaces its teeth in a different pattern and rate[68-70]. Tooth replacement and the establishment of new teeth require tooth resorption and remodeling of the tooth-bearing bones. First, the mineralized basis of the tooth must be resorbed in order to disconnect the tooth from the underlying bone[62,67,68,70-72]. Resorption of the bone creates space for the new tooth. The old tooth is completely resorbed as an alternative to shedding, perhaps to retain the minerals[66,73-75]. Therefore, from a quantitative perspective, we expect that a single, well-preserved fish specimen will possess two functional molariform teeth.

Our study on the anatomical location of *Luciobarbus longiceps* (Jordan barbel; Valenciennes 1842; SMNH#13.125) pharyngeal jaw and teeth was performed with a Micro-CT (housed at the Shmunis Family Anthropology Institute, at the Dan David Center for Human Evolution and Biohistory Research, Tel Aviv University). It revealed that the attached teeth are fully mineralized (gold color = enameloid), whereas the replacement teeth are not (blue teeth = dentin) and, therefore, will fail to be preserved following the fish's death (Extended Data Fig. 2).

It should be noted that the anatomic location of the pharyngeal teeth protects them from direct exposure to surrounding heat (Extended Data Fig. 2)[76].

C. NATURAL *VS*. CULTURAL ASSEMBLAGES OF GBY FISH REMAINS

One of the main difficulties in the analysis of fish remains from waterlogged sites is how to differentiate culturally modified fish assemblages from natural ones[8,77-84]. In this study, we applied a multivariate approach using "diagnostic signature criteria" to distinguish between natural and cultural fish assemblages (Supplementary Table 3)[80,81,83-90]. These included: fish taxonomic representation compared with the native fish community; relative taxon abundance; fish body size; body-part representation; skeletal elements fragmentation patterns; state of preservation; fish remains dispersal pattern; and mean bone scatter frequency (BSF[8,81]). Our findings indicate (Extended Data Fig. 3a; Supplementary Table 3) that the fish remains recovered from Area A reveal a high taxon richness (S' = 16) and diversity (Brillouin Index = 1.244, Fisher α = 2.359), reflecting more than 60% of the native fauna; the species represent three families of freshwater fish: Cyprinidae (carp), Cichlidae (St. Peter's fish) and Clariidae (catfish); a clumped distribution with high BSF; good preservation and presentation of skeletal elements from all anatomic regions; a wide range of body sizes of Cyprinidae and Cichlidae and an absence of medium to large-sized Clariidae (catfish). Cyprinidae remains and their pharyngeal teeth are over-represented. This reconstruction of the fish community of the paleo-Lake Hula reveals it to have been a remarkably stable habitat, featuring diverse aquatic fauna that the GBY hominins could have easily exploited throughout the year[18,27].

The above findings imply that the fish recovered in Area A (Fig. 1) were a consequence of natural fish death[27,83]. The taxonomic composition of the fish in Area A differs significantly from that recovered in Area B (χ^2 = 3748.31; df = 15; r^2 = 0.065; $p < 0.0001$), as can be observed in the correspondence analysis presented in Extended Data Fig. 4a, which separates the natural assemblage (Area A), characterized by high taxon richness, from the anthropogenic assemblages (Area B II-6 L1–7), characterized by low taxon richness (mainly two species of cyprinids: *L. longiceps, C. canis*). Overall, Area A presents a similar preservation pattern to that observed in other natural death assemblages[91,92], and it is also dominated by small and juvenile fish taxa such as *Garra rufa, G. nana, Pseudophoxinus* sp., *Acanthobrama* lissneri, and the endemic species *Mirogrex hulensis* (Extended Data Fig. 4a). The variations observed in the

morphological characteristics of the pharyngeal jaws suggested that other, as yet undescribed, species of *Acanthobrama* sp., and other small cyprinids may have also existed in the paleo-lake. In addition to the wide taxonomic diversity observed for Cyprinids, four species of Cichlidae were identified: *Oreochromis aureus*, *Sarotherodon galilaeus*, *Coptodon zillii*, and the endemic species *Tristramella simonis intermedia*[27,57].

Examination of the state of preservation of the skeletal elements revealed the over-representation of cyprinid pharyngeal teeth to be a unique local preservation-taphonomic bias. A significant difference exists between Areas A and B (II-6 L1–7) (Extended Data Fig. 4b: $\chi^2 = 6312.85$; df = 1; $p < 0.0001$, with a negative deviation of -1704), as observed from the relative abundance of bones *vs*. pharyngeal teeth. This pattern of preservation (regardless of sediment type, Supplementary Table 2) supports the conclusion that the exceptional abundance of cyprinid pharyngeal teeth in the eight superimposed AHs of II-6 L1–7 did not result from natural death, diagenesis, or the type of sediment in which the fish were deposited (Fig. 1)[4,8,27,83,88,89,93,94]. Rarefaction analysis[95] (Extended Data Fig. 3b) further supports this conclusion, indicating that the differences observed in taxonomic composition and preservation are not biased due to sample size (Supplementary Table 2). It has been demonstrated that cooking with low-moderate heat (<500 °C) softens the fish bones (leading to their rapid disintegration), yet, has minimal effect on tooth preservation[76,96-98]. We therefore posited the null hypothesis that the exceptional preservation of cyprinid pharyngeal teeth found at GBY AHs II-6 L1–7 resulted from prolonged exposure of the fish to controlled heat (and not to direct fire), manipulated by GBY hominins to cook these fish. For early hominids, fish processing by heat had many nutritional advantages, such as increasing the content of crude protein, better preservation of the nutrients, eliminating harmful parasites, and producing easy-to-digest food[99].

Supplementary Table 3. Comparison between diagnostic criteria of naturally accumulated fish remains from Lake Kinneret, and fish remains recovered from GBY Area A (AHs I-4 and I-5) and two selected archaeological horizons in Area B (II-6 L1 and II-6 L4) (after[11,12,83,86]; for GBY lacustrine sedimentological sequence by AHs, see Fig. 3.13 in[9]).

Diagnostic criteria	Natural assemblage Kinneret	GBY Area A AH		GBY Area B AH	
		I-4	I-5	II-6 L-1	II-6 L-4
Sediment	Three lithofacies of lacustrine sediments	Black mud	Coquina	Black mud	Coquina
Excavated area	12 m^2 with a max. depth of 0.5 m	5.25 m^2 with a volume of 1.57 m^3	5.00 m^2 volume of 0.55 m^3	23.79 m^2 and a volume of 4.28 m^3	16.64 m^2 and a volume of 2.16 m^3
Sample size NISP	5,037	6,014	3,192	2,644	4,827
Mean bone scatter frequency (BSF)	423 bones per 0.25 m^2 (range 8-2,840 bones)	219 elements per m^2	116 elements per m^2	22 teeth per m^2	47 teeth per m^2
Association with hearths	No	No	No	Yes	Yes
Color + burning signs	Brown (light to dark) with no signs of burning	Orange, brown and dark brown, with no signs of burning	Orange, brown and dark brown, with no signs of burning	Orange, brown and dark brown, with no signs of burning	Orange, brown and dark brown, with no signs of burning
Taxonomic composition:					
Taxon richness-S'	S' = 5	S' = 13	S' = 10	S' = 2	S'= 4
Family representation	Cyprinidae 80% Cichlidae 6% Clariidae 6%-on surface	Cyprinidae 92% Cichlidae 6% Clariidae 2%	Cyprinidae 97% Cichlidae 2.5% Clariidae 0.5%	Cyprinidae 100%	Cyprinidae 99.92% Cichlidae 0.08%
Abundant taxa*	*M. terraesanctae*, small cyprinids	*L. longiceps* 31.5% *M. hulensis* 24.0% Clariidae 17.0%	*L. longiceps* 69.2% *M. hulensis* 5.3% Clariidae 6%	*L. longiceps* 61% *C. canis* 39%	*L. longiceps* 86% *C. canis* 14%
Skeletal representation:					
Skeleton richness	55	58	35	1	1
Scales	Clumps of scales in all taphofacies	none	none	none	none
Otoliths	No otoliths	No otoliths	No otoliths	No otoliths	No otoliths
Crania vs. postcrania:					
Cyprinidae	Cranial region is over-represented	Cranial region & pharyngeal teeth are over-represented >85%	Cranial region & pharyngeal teeth are over-represented >93%	Pharyngeal teeth 100%	Pharyngeal teeth 100%
Cichlidae	Cranial region is under-represented	Cranial region is under-represented	Cranial region is under-represented	None	None

D. TOOTH MINERAL COMPOSITION: XRD ANALYSIS

The primary mineral of bone, as well as tooth dentin and enamel, is hydroxylapatite (HAp), idealized as: $Ca_5(PO_4)_3(OH)$. Studies have shown that in cartilaginous fish, the enameloid is of ectomesenchymal origin with fluorapatite as the mineral phase $Ca_5(PO_4)_3F$. All other groups form enamel of ectodermal origin, using hydroxylapatite as the mineral phase[70,100-103]. Chemical analysis revealed that since they contain ions of carbonates (CO_3), with variations in mineral content of HPO_4, F, Cl, Mg, Na, K, and some trace elements of Sr and Zn, this biogenic HAp is considered as carbonated apatite[103-108].

Bone and dentin are organically rich (> 20%), highly porous, poorly crystalline, and feature tiny nanometer-sized crystals (20 x 4 nm)[109-111]. The crystal structure of apatite is hexagonal, displaying preferred *c*- axis and *a(b)*- axis orientation, respectively, when the *c*- axis orientation is very close to horizontal (perpendicular to the tooth occlusal surface)[111-114]. Consequently, due to post-mortem diagenetic alteration they often undergo extensive processes of recrystallization and-alterations[115,116]. As a result, carbonate is incorporated into the bone or dentin, either substituting as CO_3 for PO_4 (Type B) with charge balancing substitution of Na for Ca, or substituting as CO_3 for OH (Type A)[117]. The tooth enamel is the hardest tissue covering the tooth crown surface. It consists of 96% (wt) inorganic mineralized material, 1% (wt) organic material, and 3% (wt) water and is less prone to recrystallization[109]. The enamel is, therefore, less susceptible to recrystallization and is resistant to diagenetic alteration[105,115,116,118-121]. Moreover, if enamel recrystallization takes place, this leads to fluorine uptake and the formation of carbonated fluorapatite, although the composition of the structural carbonate is often unaffected and retains its original isotopic composition[103-105,112,115-118].

X-ray diffraction (XRD): XRD measurements have been widely used as a conventional technique to determine lattice parameters in crystalline structures and to assess crystallinity (crystallite size = CS). Studies have shown that changes to the microstructure of bone and teeth occur during heating, suggesting that higher temperatures increase crystallite size and decrease crystal strain[122,123]. The advantage of the X-

ray diffraction (XRD) technique has been amply demonstrated for identifying heat-induced changes in bones and teeth[123-127].

Measurement conditions: The XRD was set up in Bragg-Brentano geometry using a copper X-ray source, sample spinner, nickel filter, and X'celerator detector. Tube operation conditions were 45 kV and 40 mA. Primary and secondary Soller slits of 0.02 rad were used, and the divergence slit was set to 0.25°. The measurements were carried out between 5 and 120° 2θ at a step size of 0.017° and a time per step of 200 s to 400 s. The samples were rotated during the measurements to increase the number of crystallites in the X-ray beam to obtain a better powder average.

LaB_6 (NBS 660a) was used as an external standard and analyzed under the same conditions as the samples. The HighScore Plus software (Panalytical) was used for the crystallite size and microstrain analyses.

Size and strain were refined using the Rietveld method. The peak profiles were modeled using a pseudo-Voigt function. The instrumental contributions to the peak profiles were fitted with the LaB_6 standard, including refinement of the Cagliotti parameters *U*, *V*, and *W*. For the size-strain analysis of the samples, we fixed the *V* parameter to the standard value and refined *U* and *W* as well as the unit cell parameters. Refined global parameters were sample displacement and background (polynomial function). The apatite crystal structure of Hughes et al.[128] (ICSD code 203027) was used as a starting model. Whitlockite was identified as a secondary phase at high temperature (calcified state), and the structure data of whitlockite were taken from Schroeder et al.[129] (ICSD code 6191).

Assess effects of diagenesis on crystallite size: To increase our understanding of the effect of diagenetic alteration during natural fossilization processes on crystallographic parameters of fish teeth enameloid, we incorporated data published on paleontological fish teeth[113,114,130,131]. Estimation of the diagenetic processes through time was performed using an interpolation curve that examines the effect of carbonate substitutions, with changes observed in the lattice parameters *a* and *c*. Studies have revealed that the parameter ratio *c*/*a* can be used to estimate the carbonate content in B-type HAp (as stoichiometric coefficient value x). This curve was fitted to the following equation[132]:

stoichiometric coefficient (x) = 6x(30.383x c/a - 22.208)[3/4]

We applied this calculation to the lattice parameters *a* and *c* obtained for the teeth examined in this study (Supplementary Table 4). For comparison, we added values from published data on fossil fish teeth from the last 450 million years[113,130,131] (Extended Data Fig. 5a and b). The data confirm that the carbonate content in the apatite structure of teeth increases with time[122]. However, the crystallite size seems to be unaffected by carbonate substitution. For instance, the mean crystallite size of unheated fresh Cyprinidae teeth (16.5 ± 1.3 nm) and the 4–3.15 Mya old of Erq-el-Ahmar (16.4 ± 1.4 nm) are similar (Extended Data Fig. 5c).

We examined the relation between enameloid microstrain and CS under different heating conditions (ranging between 200 and 600 °C), and compared the results to the values obtained for fossil cyprinid teeth (GBY and Erq-el-Ahmar; Extended Data Fig. 5). We show schematically (Extended Data Fig. 5c and d) that when cooked at a temperature above 500 °C, CS increases whereas microstrain sharply decreases.

The alteration patterns observed in this study strengthen our conclusion that the CS increase found in GBY fish teeth enameloid was due to heating and not caused by low-temperature diagenetic alterations in the sediment (Extended Data Fig. 5c and d). Moreover, it raises the possibility that if diagenetic changes did take place in the GBY fish tooth enameloid, this could have reduced the CS, thus somewhat challenging our ability to identify heat-induced changes. Nonetheless, despite the difficulty in identifying evidence of cooking at low heat, we could detect heat-induced changes in CS in ca. 40% of the *L. longiceps* molariform teeth at GBY.

Supplementary Table 4. Parameters calculated for *L. longiceps* and *M. piceus* teeth enameloid examined in the current study by XRD.

Site	Tooth catalogue no.	Temp (°C)	Cooking time	*a* (Å)	*c* (Å)	*V* (Å^3)	CS (nm)	Micro strain [%]	*c/a*
GBY (Area)									
A	#5052			9.4218(11)	6.8846(9)	529.3(1)	16.3(3)	0.41(1)	0.7307
A	#5642			9.4180(13)	6.8864(10)	529.0(1)	16.7(3)	0.43(1)	0.7312
A	#12664			9.4149(14)	6.8855(11)	528.5(1)	14.2(2)	0.46(1)	0.7313
B	II-6 L1 #30008			9.4087(13)	6.8840(10)	527.8(1)	14.2(2)	0.40(1)	0.7316
B	II-6 L2 #49			9.4194(11)	6.8899(9)	529.4(1)	18.4(3)	0.31(1)	0.7314
B	II-6 L2 #605			9.4021(16)	6.8860(12)	527.2(2)	15.6(3)	0.37(1)	0.7324
B	II-6 L2 #1256			9.4120(13)	6.8877(10)	528.4(1)	17.8(3)	0.36(1)	0.7318
B	II-6 L2 #82			9.4155(10)	6.8880(8)	528.8(1)	20.3(3)	0.40(1)	0.7315
B	II-6 L2 #6F			9.4080(11)	6.8876(9)	527.9(1)	17.3(3)	0.34(1)	0.7321
B	II-6 L2 #228			9.4179(11)	6.8865(9)	529.0(1)	19.4(4)	0.34(1)	0.7312
B	II-6 L3 #63041			9.4244(14)	6.8878(8)	529.8(1)	16.8(2)	0.33(1)	0.7311
B	II-6 L3 #65600			9.4125(10)	6.8861(8)	528.3(1)	16.5(2)	0.36(1)	0.7318
B	II-6 L3 #66757			9.4146(10)	6.8823(8)	528.3(1)	15.1(2)	0.40(1)	0.7310
B	II-6 L4 #67272			9.3888(11)	6.8900(8)	526.0(1)	16.3(2)	0.32(1)	0.7339
B	II-6 L4 #69255			9.4207(8)	6.8894(6)	529.5(1)	20.4(3)	0.33(1)	0.7313
B	II-6 L4 #69252			9.3983(11)	6.8914(8)	527.1(1)	14.6(2)	0.38(1)	0.7458
B	II-6 L6 #468			9.4130(14)	6.8894(8)	528.6(1)	17.5(3)	0.38(1)	0.7319
B	II-6 L6 #30007			9.4146(12)	6.8875(9)	528.7(1)	18.4(3)	0.36(1)	0.732
B	II-6 L6 #200,001			9.4146(10)	6.8874(8)	528.7(1)	16.9(2)	0.40(1)	0.7316
B	II-6 L6 #84000			9.4126(12)	6.8876(10)	528.5(1)	17.1(3)	0.38(1)	0.7317
B	II-6 L6 #84001			9.4196(10)	6.8902(8)	529.5(1)	18.2(3)	0.34(1)	0.7315
B	II-6 L6 #469			9.4097(13)	6.8841(10)	527.9(1)	15.7(3)	0.41(1)	0.7316
B	II-6 L6 #484			9.4187(9)	6.8878(7)	529.2(1)	20.2(3)	0.33(1)	0.7312
B	II-6 L6 #100,000			9.4131(12)	6.8859(9)	528.4(1)	16.0(2)	0.36(1)	0.7315
B	II-6 L6 #485			9.4241(9)	6.8880(7)	529.8(1)	20.7(3)	0.30(1)	0.7308
B	II-6 L7 #30002			9.4215(11)	6.8855(8)	529.3(1)	18.3(3)	0.35(1)	0.7308
B	II-6 L7 #30003			9.4156(12)	6.8829(9)	528.4(1)	15.0(2)	0.36(1)	0.7310
B	II-6 L7 #87374			9.4134(8)	6.8843(6)	528.3(1)	19.3(3)	0.34(1)	0.7313
B	GBYB #125			9.3886(20)	6.8885(16)	525.8(2)	14.2(3)	0.39(2)	0.7337
PALEO									
ERQ	#30005			9.4137(12)	6.8873(10)	528.6(1)	16.5(3)	0.35(1)	0.7316
ERQ	#30005b			9.4096(10)	6.8855(8)	528.0(1)	17.8(3)	0.33(1)	0.7317
ERQ	#30005c			9.3895(11)	6.8865(8)	525.8(1)	14.9(2)	0.40(1)	0.7334
FRESH									
	L. longiceps #430			9.4441(8)	6.8878(6)	532.0(1)	17.1(2)	0.30(1)	0.7293
	L. longiceps #222			9.4483(8)	6.8871(6)	532.4(1)	17.2(2)	0.30(1)	0.7289
	M. piceus #10/1			9.4522(11)	6.8892(9)	533.0(1)	17.0(3)	0.30(1)	0.7288
	M. piceus #10/3			9.4508(12)	6.8894(9)	532.9(1)	17.2(3)	0.28(1)	0.7289
	M. piceus #11/1			9.4515(9)	6.8929(9)	533.2(1)	16.9(2)	0.30(1)	0.7293
	M. piceus #11/2			9.4582(17)	6.8840(13)	533.3(2)	13.9(2)	0.53(1)	0.7278
OVEN HEATED									
	M. piceus 12a	200	4 hours	9.4459(9)	6.8840(7)	531.9(1)	18.7(2)	0.34(1)	0.7287
	M. piceus 12b	200	4 hours	9.4462(8)	6.8854(6)	532.1(1)	20.4(3)	0.34(1)	0.7289
	M. piceus 12c	200	8 hours	9.4448(10)	6.8847(8)	531.9(1)	18.7(3)	0.34(1)	0.7289
	M. piceus 10a *	200	1 hour	9.4440(11)	6.8868(8)	531.9(1)	17.4(3)	0.35(1)	0.7292
	M. piceus 10b*	200	8 hours	9.4419(10)	6.8873(8)	531.7(1)	17.5(3)	0.34(1)	0.7294
	M. piceus 11b	250	2 hours	9.4388(11)	6.8895(9)	531.6(1)	16.8(3)	0.30(1)	0.7299
	M. piceus 11c	300	4 hours	9.4385(8)	6.8886(6)	531.4(1)	19.2(2)	0.31(1)	0.7298

Supplementary Table 4. *Cont.*

FIRE COOKING									
	M. piceus 3	400	30 min at 300 °C & 45 min at 400 °C	9.4506(10)	6.8911(8)	533.0(1)	18.5(3)	0.30(1)	0.7292
	M. piceus 3	400	30 min at 300 °C & 45 min at 400 °C	9.4533(11)	6.8894(8)	533.2(1)	16.7(2)	0.31(1)	0.7287
	M. piceus 3a	400	30 min at 300 °C & 45 min at 400 °C	9.4512	6.8871	532.8	16.6	0.33	0.7287
	M. piceus 3b	400	30 min at 300 °C & 45 min at 400 °C	9.4543	6.8879	533.2	16.5	0.37	0.7285
	M. piceus 8	500	30 min at 300 °C & 45 min at 500 °C	9.4509(9)	6.8924(7)	533.1(1)	17.9(2)	0.24(1)	0.7292
	M. piceus 7	600	30 min at 300 °C & 45 min at 600 °C	9.4384(8)	6.8912(7)	531.7(1)	22.2(4)	0.20(1)	0.7301
	M. piceus 6	700	30 min at 300 °C & 45 min at 700 °C	9.4471(6)	6.8882(5)	532.4(1)	32.9(7)	0.19(1)	0.7291
	M. piceus 5	800	30 min at 300 °C & 45 min at 800 °C	9.4759(4)	6.8799(4)	534.9(1)	40.2(9)	0.21(1)	0.7260
	M. piceus 2	900	30 min at 300 °C & 45 min at 900 °C	9.4824(3)	6.8793(3)	535.7(1)	68.2(22)	0.14(1)	0.7254
	M. piceus 4	900	30 min at 300 °C & 45 min at 900 °C	9.4734(5)	6.8759(5)	534.4(1)	51.9(18)	0.16(1)	0.7258

CS = Crystallite Size (= Crystallinity Index); ERQ = Erq-el-Ahmar
*Powdered enameloid = crushed powdered enameloid prepared for the XRD sample.
Complete fish cooked in the fire are listed under "fire cooking".
Isolated fish teeth were heated in the lab oven.
Values in brackets are estimated standard deviations and refer to the last decimal places.

Statistical analysis of the crystallite size (CS) of Cyprinidae molariform teeth:

To determine the threshold between uncooked (raw) and cooked fish, we compared CS in three groups that were exposed to various temperatures: fresh uncooked fish or fish heated at low temperatures (< 200 °C), fish cooked at moderate temperatures (200–500 °C), and fish cooked at high temperatures (> 600 °C). The teeth from GBY were classified into two groups: those recovered from Area A (natural death assemblage) and those recovered from the eight sequential AHs of Area B (II-6 L1–7) (Supplementary Table 5).

Examination of enameloid CS (Supplementary Table 5) in the various groups showed that CS in teeth from Area A and fresh unheated fish did not exceed 17.2 nm; CS in teeth of fish cooked at moderate temperatures (200–500 °C) displayed a larger range, between 16.5–20.4 nm; CS in fish cooked at high temperatures (> 500 °C) exceed 23 nm. At GBY teeth from Area A displayed low CS, similar to the values of unheated fish.

However, teeth from Area B II-6 L1–7, however, displayed a wider range (14.2–20.7 nm), while 11 teeth displayed CS of 18.2–20.7 nm, similar to CS of fish cooked at moderate heat (Fig. 3; Supplementary Table 4).

Non-parametric Wilcoxon pair comparison was carried out to test for significant differences in CS between the different groups sampled (teeth from GBY Area B II-6 L1–7, and from GBY Area A, fresh unheated teeth, and heated fish [below and above 500 °C]). The results revealed the following: CS of teeth from Area A was significantly smaller than CS of teeth exposed to moderate and high heat; CS of teeth from Area B differed significantly from CS of teeth exposed to high temperature (> 500 °C) (Supplementary Table 6; Fig. 3).

These analyses confirmed that at GBY *L. longiceps* molariform teeth with CS above 18 nm had undergone heat-induced changes in apatite crystallite size (i.e. CS increase), but had not been exposed to high heat (> 500 °C). All these teeth were recovered from the eight sequential AHs of Area B (II-6 L1–7).

Supplementary Table 5. Cyprinidae molariform pharyngeal teeth enameloid crystallite size (nm) ([CS] range, mean, median, mode, and standard deviation [Std. Dev.]), grouped according to heating temperatures and by excavated areas at GBY.

Pharyngeal Teeth Group	NISP	Mean CS (nm)	Std. Dev.	Range (nm)	Median	Mode
Fresh unheated fish	6	16.55	1.30	13.9 – 17.2	16.3	17.2
Cooked at moderate heat 200–500 °C	12	17.91	1.21	16.5 – 20.4	17.7	18.7
Cooked above 500 °C (burnt)	5	43.08	17.72	22.2 – 68.2	40.2	-
GBY A (natural death)	3	15.73	1.34	14.2 – 16.7	16.3	-
GBY B II-6 L1–7	25	17.54	1.93	14.2 – 20.7	17.5	18.4

E. SPATIAL ANALYSES OF FISH REMAINS AND BURNT FLINT MICROARTIFACTS

Excavation methods and provenance recording: Excavations at GBY were carried out using a horizontal 1 sqm grid constructed above the excavated surfaces and corresponding to the coordinates of the Israeli grid. Excavations were conducted along the strike and dip of the geological layers with the aim of laterally exposing the tilted AH (Extended Data Fig. 1d)[9]. This procedure enabled a detailed representation of the

spatial organization of each AH[26]. The standard excavation unit was thus the tilted projection of a horizontal 1 m^2 grid square. Each horizontal grid square was subdivided into four 0.5 × 0.5 m sub-squares and excavated in spits that covered the area of one sub-square to an average depth of 5 cm. Following exposure, the surface was drawn and items were retrieved with a full spatial reference (X, Y, and Z). These "coordinated pieces" mainly comprised items larger than 20 mm (i.e. macro-artifacts). Other items retrieved during the excavation—the "uncoordinated pieces"—were labeled according to the spit's spatial reference (i.e., the excavated unit/sub-square and an elevation range). Such items can thus be located to a precision of 0.5 × 0.5 × 0.05 m.

In addition to material retrieved during the excavation, the excavated sediments embodying the AHs were wet sieved at the site using a 2 mm sieve. The sediments were then bagged with their recorded spit location and transported to the Institute of Archaeology at the Hebrew University for further analysis. Sorting the sieved sediments yielded rich and varied assemblages, including fruits, seeds, grains, bones and teeth of micro-vertebrates, mammals, fish, crabs, lithic microartifacts (2 to 20 mm; basalt, flint, limestone), and specks of charcoal[9,18-21,27-29,57,133].

Spatial plotting: A large amount of archaeological material was retrieved under a general spatial reference, either during the excavations or through the sorting of the wet-sieved sediments. The sediments' spatial reference includes the X and Y quadrant (0.5 × 0.5 m) and the spit depth (Z is a range of depths). Only such spatial recording enables the representation of relative frequencies per excavated unit. Other spatial analyses, such as creating a density map or performing hotspot analysis, would necessitate measuring the distances between different features and thus require that the data be depicted as distinct points.

It has been suggested that assigning a random spatial reference within the excavated area provides a reliable and almost identical spatial representation[134]. Considering this and using the *Visual Basic* language within the *Access* program (Microsoft® Access 2016), items with a general spatial reference were given a new reference point within their recorded sub-square. This procedure enabled the plotting of each excavated find and comprised several stages.

First, each database (of the different finds categories) was treated separately and sorted according to the recorded excavated units. Each of these units featured a defined excavated area (0.5 × 0.5-m sub-squares or 1 × 1-m squares), from which a certain number of items was retrieved. This area (a) was then divided by the maximum number of items retrieved from that area (n) so that each item could be plotted separately within an a/n area (δ). Hypothetically: if a given 1 m^2 excavated area (a = 1) contains 100 flint items (n = 100), and if these 100 items were distributed *evenly* within the 1 m^2 area, each item would then occupy an area of 1/100 m^2 (δ = 0.01). The new reference point for each item is thus defined as the south-western corner of each δ cell, so that:

$$a = \sum \delta_{1\text{-}n} \, (\delta_1+\delta_2+\delta_3+\delta_4 \ldots \delta_n)$$

This procedure enables the items to be plotted *uniformly* within their recorded spit, ensuring that the new plotted data are as consistent as possible with the recorded data of sub-square precision. Other plotting methods (e.g., random plotting) could result in the formation of artificial clusters within the sub-square area.

The assignment of artificial coordinates to the archaeological material enables the various databases to provide geographical information that can be integrated into GIS software. This package is a collection of software and geographic data for capturing, managing, analyzing and displaying all forms of geographically referenced information (see: http://www.esri.com/software/arcgis/about/desktop_gis.html).

Kernel density calculates the density of point features around each output cell (determined here as 0.01 m). Conceptually, a smoothly curved surface is fitted over each point. The surface value is highest at the location of the point and diminishes with increasing distance, reaching 0 at the search radius distance from the point (determined here as 0.5 m). Consequently, only a circular neighborhood is possible. The density value at each output cell is calculated by adding the values of all the kernel surfaces where they overlie the cell center[135]. Determination of different search radii thus alters the scale of the analysis results. With a smaller radius, fewer points will fall within the search radius, resulting in numerous small "dense" features.

Increasing the radius will result in more points falling within the search radius. When calculating density, the number of points will be divided by a larger area, leading to larger, generalized concentrations. The cell size (0.01 m) and search radius (0.5 m) values were chosen for this study since they closely represent the actual patterns observed within the schematic illustrations of the data (i.e. frequencies per excavated unit/sub-square). Finally, in order to create a uniform scale (from 0 to 1) enabling comparison between kernel density maps of different datasets (e.g., burnt vs. unburnt flint; burnt flint vs. fish remains), the densities were standardized according to the maximum values of each dataset.

Previous analyses of the burnt and unburnt flint microartifacts from the entire occupational sequence at GBY have established evidence of the controlled use of fire. That conclusion was based on the presence of clusters of burnt flint that did not overlap with those of the unburnt flint (tested statistically using Homogeneity Analysis), chi-square (χ^2) tests, and standardized residuals (SR)[16,26,35,37,39]. In addition, a study combining spatial analysis and thermoluminescence (TL) analysis demonstrated that the TL signal from flint microartifacts close to the hearth's center revealed unambiguous signs of moderate heating (< 500 ˚C), whereas with increasing distance from the hearth, the TL signal can be interpreted as a result of decreasing temperatures and/or shorter durations of exposure to fire[39]. A few charred wood pieces were spatially identified in the hearths[26], providing indication of the fueling agent. The presence of driftwood at all AHs[133] further supports the notion that wood was the primary source of energy for the hearths.

The spatial analysis of the fish remains from GBY followed the same methodology used to map the burnt flint microartifacts. These density maps (Supplementary Fig. 1) illustrate the clustering of fish remains in the eight AHs of Area B and their spatial association with clusters of burnt flint microartifacts. The statistical significance of the clustering of fish remains was evaluated using the 'Optimized Hot Spot Analysis' tool, available in the spatial statistics package of *ArcMap* (ESRI®ArcMap™9.3). The optimized hot spot analysis creates a map of statistically significant hot and cold spots using the Getis-Ord Gi statistic. It evaluates the characteristics of the input data (i.e., the spatial location of fish remains) to produce optimal results. The data aggregation method used was 'Snap Nearby Incidents' to create weighted points. In this

method, nearby incidents are aggregated together to create a single weighted point. The weight for each point is the number of aggregated incidents at that location. The results of the optimized hot spot analysis suggest that the clustering of fish remains is statistically significant in each of the studied archaeological horizons (Supplementary Fig. 2) with confidence levels of 90% (z-score > 1.65, p-value <0.10), 95% (z-score > 1.96, p-value < 0.05), and 99% (z-score > 2.58, p-value < 0.01).

Supplementary Fig. 1: Kernel density maps (on a uniform scale between 0 – 1) of burnt flint microartifacts (red) and fish remains (blue) from GBY Area B Archaeological Horizons II-6 L1–7.

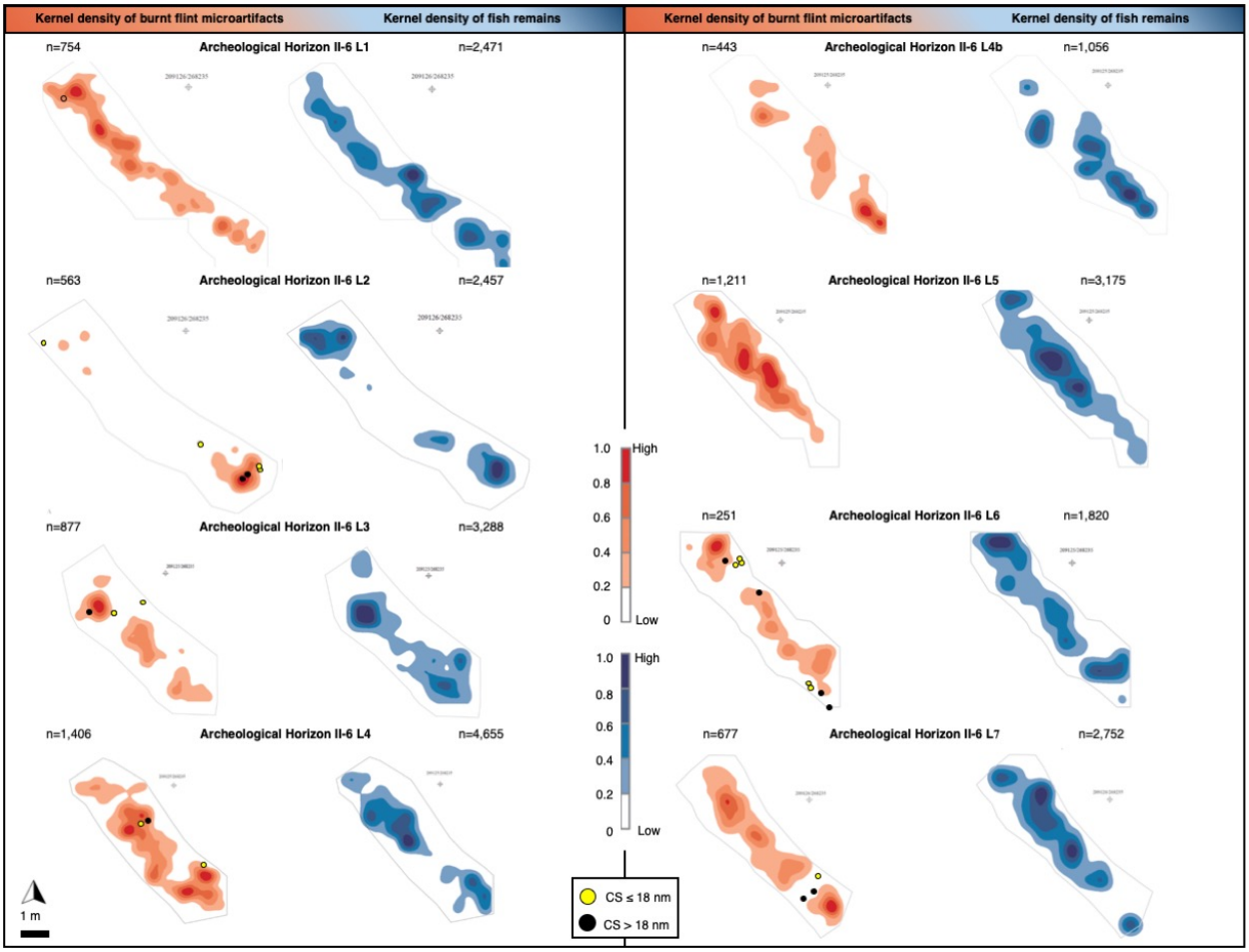

Kernel density maps of burnt flint microartifacts (red) and of fish remains (blue) in GBY Area B AHs II-6 L1-7 (the darker the color, the greater the density). The maps exhibit the overlap between clusters of burnt microartifacts (left) and those of fish remains (right). Pharyngeal teeth with an enameloid CS value smaller than 18 nm are marked as yellow dots, and those with CS larger than 18 nm are marked as black dots (data in Supplementary Table 4).

Supplementary Fig. 2: **Optimized hotspot analysis of fish remains from GBY Area B Archaeological Horizones II-6 L1–7.**

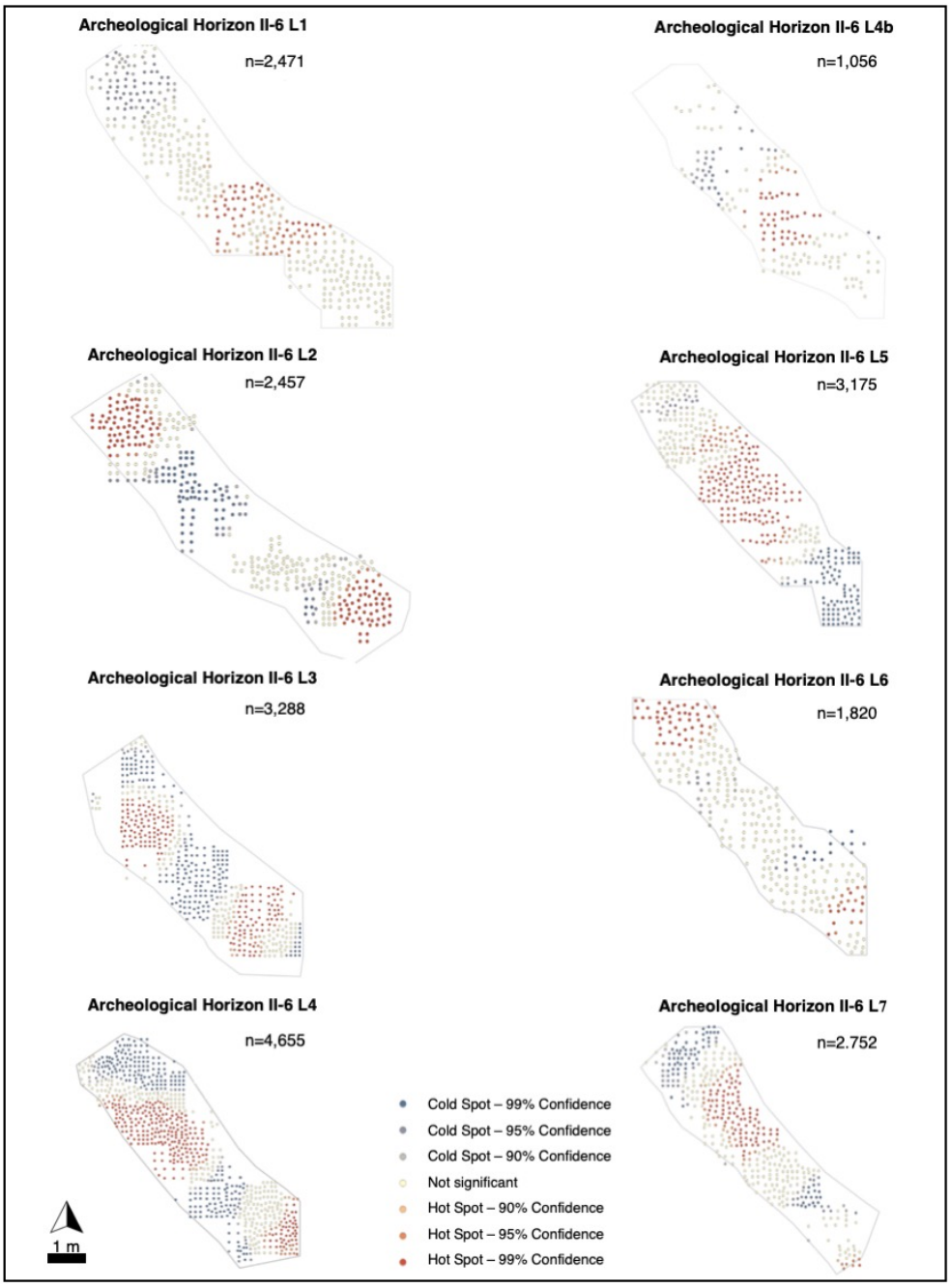

The optimized hot spot analysis suggests that the clustering of fish remains is statistically significant in each of the AH associated with controlled heat, with confidence levels of 90% (z-score > 1.65, p-value < 0.10), 95% (z-score > 1.96, p-value < 0.05), and 99% (z-score > 2.58, p-value < 0.01).

F. STABLE OXYGEN AND CARBON ISOTOPE ANALYSES OF FISH TEETH

Fish bones and teeth are mineralized in oxygen isotope equilibrium with the body fluid. The body fluid of fish has the same oxygen isotope composition as the ambient water ($\delta^{18}O_{Water}$), and the body (i.e. tooth formation) temperature of fish is identical to the ambient water temperature. Thus, the bioapatite $\delta^{18}O_{PO4}$ and $\delta^{18}O_{CO3}$ values of fish are controlled by the $\delta^{18}O_{Water}$ value and the water temperature according to the temperature-dependent water-phosphate oxygen isotope fractionation[136-139]. Fish bioapatite $\delta^{18}O_{PO4}$ and $\delta^{18}O_{CO3}$ values thus offer a powerful proxy to infer past fish habitats and season of capture[115,116,140-146].

Lake water oxygen isotopic composition is controlled by several variables, including seasonal changes in temperature, precipitation, air mass trajectory, and the rate of evaporation and groundwater flux[147-149]. In the Jordan Rift Valley, the stable isotope records reflect phases of low lake levels and evaporative enrichment that may lead to saline conditions, alternating with periods of increased precipitation and chemically diluted water flux[147-149]. Previous studies of Rift Valley Lake sediments have demonstrated the effect of evaporation on progressive ^{18}O-enrichment of lake water. Moreover, the isotopic signature differs between the aquatic habitats from north to south: the Dan River and Lake Hula in the north revealed a mean $\delta^{18}O_{water}$ of -7.5‰ increasing to -3‰ in the lower Jordan River, between -2.5 to 0.0‰ in Lake Kinneret, and reaching over +4‰ in the Dead Sea[148-152].

In biogenic apatite (carbonate-hydroxylapatite), oxygen is present in three different moieties within the crystal structure: in the phosphate, carbonate, and hydroxyl groups. Measurements of the carbonate fraction of biological apatite provide two simultaneous ecological proxies ($\delta^{18}O$ and $\delta^{13}C$). However, due to the strength of the P-O bonds, $\delta^{18}O_{PO4}$ values of the phosphate group are considered to be more resistant in fossils to post-mortem alteration than those of the carbonate group and are therefore regarded as an "ideal geochemical recorder" of the environmental conditions during the organism's life before death[138,153,154]. Recent studies have demonstrated that whereas in bone and dentin the hydroxylapatite carbonate value changes due to diagenesis, in enameloid it retains the original values, reflecting environmental conditions prior to the vertebrate´s death[115,116,118,155-157]. Therefore, to test for diagenesis, we measured the spacing

between the $\delta^{18}O$ of the carbonate and phosphate fractions in the fish teeth enameloid samples and compared it to the $\delta^{18}O_{PO4}/\delta^{18}O_{CO3}$ relationship established for modern taxa[144,156].

Analyses of both the phosphate and the carbonate fraction isotope composition ($\delta^{18}O_{PO4}$, $\delta^{18}O_{CO3}$, and $\delta^{13}C$) were performed on 27 molariform teeth of *L. longiceps* from different areas of GBY: Area A (n = 4), Area B (n = 21), and Area C (n = 2) (Supplementary Table 6; Extended Data Fig. 6). For comparison, we analyzed molariform teeth of modern cyprinids caught in different freshwater habitats of the Rift Valley: Jordan River (n = 2), Lake Kinneret (n = 4), and *L. longiceps* molariform teeth from the Lower Paleolithic site of 'Ubeidiya (n = 9), located 3 km southeast of Lake Kinneret (Extended Data Fig. 1a). The lacustrine conditions in paleo-lake 'Ubeidiya represent a freshwater paleo-lake with sequential changes in water salinity level and temperature[7,158-160].

The phosphate fraction of the samples were separated using a method modified after Dettmann *et al.*[161] and described in detail by Tütken *et al.*[162] and Sisma-Ventura *et al.*[145]. The carbonate fraction determination followed Sisma-Ventura *et al.*[144]. Approximately 5 mg of pre-treated sample powder was digested in 0.8 ml HF (2 M) on a vibrating table for ca. 12 h. Following centrifugation, the supernatant sample solution was separated from the CaF precipitates into a new vial. After neutralizing the HF solution with NH_4OH (25%) in the presence of bromothymol blue as pH indicator, Ag_3PO_4 was precipitated by adding 0.8 mL of 2 M $AgNO_3$. After settling of the Ag_3PO_4 crystals, the samples were centrifuged, and the supernatant solution containing excess $AgNO_3$ was removed using a pipette. The Ag_3PO_4 precipitate was then rinsed five times with Milli-Q water and dried overnight in an oven at 50 °C. Ag_3PO_4 aliquots of 0.5 mg were placed in silver capsules and analyzed in triplicate by means of high-temperature reduction using a Finnigan TC-EA coupled via a Conflo III to a Micromass 100 GC-IRMS at the University of Mainz, or to a Finnigan Delta Plus XL GC-IRMS at the Universities of Tübingen and Lausanne, according to the method of[163]. The raw $\delta^{18}O_{PO4}$ values were normalized to an Ag_3PO_4 reference material produced by Elemental Microanalysis with a certified value of 21.7‰ (silver phosphate P/N IVA33802207, batch no. 180097, distributed by IVA

Analysentechnik, Germany). The analytical precision for this reference material was better than ±0.3‰ (1σ).

Since the $\delta^{18}O$ of the carbonate fraction in tooth enameloid is considered more prone to diagenetic alteration than the phosphate fraction[118], we first explored the spacing between $\delta^{18}O_{CO3}$ and $\delta^{18}O_{PO4}$ in modern and fossilized cyprinid enameloid samples (Fig. 6a). The $\Delta^{18}O_{CO3\text{-}PO4}$ values of ancient cyprinid teeth ranged between 7.4–12.6‰ (average 9.3±1.54‰, n = 38), similar to the $\Delta^{18}O_{CO3\text{-}PO4}$ values obtained for modern cyprinid and shark teeth (range 7.2–11.8‰; mean: 9.1±1.5‰; n = 12)[163], and modern fish teeth from the Mediterranean Sea (9.5 ± 0.7‰; n = 8)[144] (Fig. 6a).

The paired $\delta^{18}O_{PO4}$-$\delta^{13}C$ and $\delta^{18}O_{CO3}$-$\delta^{13}C$ values obtained for paleo-Lake 'Ubeidiya (1.5 Mya), and modern Lake Kinneret (Fig. 6b; Extended Data Fig. 6) indicate an intensive interplay between rate of evaporation and rate of freshwater input-precipitation, implying a higher range of water temperatures and salinity level during the year compared to the more humid conditions of paleo-Lake Hula (Discriminant analysis, Supplementary Table 7). At GBY, the $\delta^{18}O_{PO4}$ values of the cyprinid fish teeth from both Area A and the eight AHs of Area B (Fig. 6b), displayed wide ranges, thus reflecting seasonal changes in lake water temperature and hydrology. In AHs II-6 L7, fish teeth displayed a $\delta^{18}O_{PO4}$ range similar to that of $\delta^{18}O_{CO3}$ for GBY fossil freshwater gastropods from the same layer[164].

The $\delta^{18}O_{PO4}$ values of Area A significantly differed from those of the eight sequential layers of Area B (II-6 L1–7; Tukey HSD, all pairwise comparison; $p < 0.02$; Supplementary Table 8), representing in Area A fish remains of a natural death during winter[83]. The intra-layer variability in $\delta^{18}O$ values at AHs II-6 L1–7 (Fig. 6b; Extended Data Fig. 6) suggests that fish exploitation at GBY was not a seasonal activity but occurred all year round: some layers (e.g., II-6 L1) suggest fishing activities in winter and spring (i.e., cooler/wetter season), while others (II-6 L3 and L5) represent warmer/drier seasons.

Assessing the diagenetic alteration of fish tooth enameloid stable isotope compositions

Stable isotope compositions of structurally-bound CO_3 in the enamel of experimentally heated teeth remain unaltered for $\delta^{13}C$ (up to 700 ˚C) and $\delta^{18}O_{CO3}$ (up to 300 ˚C), while still falling within the range of the original values of unheated teeth[165]. Similarly, the original $\delta^{18}O_{PO4}$ values are preserved if a bone is heated up to 300 ˚C[157]. Above 300 ˚C, however, heat-induced thermal alteration occurs for $\delta^{18}O_{CO3}$ values in enamel[165] and $\delta^{18}O_{PO4}$ in bone[157]. In both cases, $\delta^{18}O$ values decrease systematically to several per mil (‰) lower values due to oxygen isotopic exchange with air humidity and/or the enamel bioapatite hydroxyl group. In contrast, the enamel $\delta^{13}C$ value remains unaltered even up to 700 ˚C[166]. As GBY fish teeth from those AHs possessing hearth structures were heated to moderate temperatures of 200–500 ˚C, their original enameloid carbon and oxygen isotope composition should still be preserved. Thus, regarding the paleohydrology of paleo-Lake Hula, inferences based on enameloid $\delta^{13}C$ values of the GBY fish teeth are clearly not biased by any heating effects. The oxygen bound in the PO_4 group ($\delta^{18}O_{PO4}$) is due to the high P-O bond strength being more robust against diagenetic alteration than that of the CO_3 group ($\delta^{18}O_{CO3}$) and, by implication, also against heat-induced changes. However, even the original $\delta^{18}O_{CO3}$ values still seem to be preserved, which is supported by the fact that most of the analyzed enameloid samples of fossil fish teeth from GBY fall within the $\Delta\delta^{18}O_{CO3}$-$\delta^{18}O_{PO4}$ array of modern bioapatite samples (Fig. 6c)[156]. Only two samples of the natural fish death assemblage from Area A fall below the $\Delta\delta^{18}O_{CO3}$-$\delta^{18}O_{PO4}$ array, as do two fish teeth from Area B AHs (60016 from LII-6 L1 and 83261 from LII-6 L7). For these teeth, therefore, some diagenetic alteration cannot be excluded. However, the taphonomically more robust $\delta^{18}O_{PO4}$ values of fossil fish teeth from both Area A (natural death) and Area B II-6 L1–7 AHs are similar and display the same range of $\delta^{18}O_{PO4}$ values (Fig. 5b). Hence, only the taphonomically robust enameloid $\delta^{18}O_{PO4}$ values are used herein to assess the fish exploitation season by GBY hominins, and thus to present reliable results.

Supplementary Table 6. Results of stable isotope analyses of modern and fossilized fish teeth (enameloid).

Sample	Collection area	Species	$\delta^{18}O_{PO4}$ (‰) VSMOW	std	$\delta^{18}O_{CO3}$ (‰) VSMOW	$\delta^{13}C_{CO3}$ (‰) VPDB	$\Delta^{18}O_{CO3\text{-}PO4}$
Modern fish teeth							
Carp [970 g]	Lake Kinneret	*C. carpio*	21.7	0.3	30.5	-6.2	8.9
Carp	Lake Kinneret	*C. carpio*	21.7	0.3	30.8	-5.2	9.1
Carp [930 g]	Lake Kinneret	*C. carpio*	21.0	0.3	30.5	-6.2	9.5
Carp	Lake Kinneret	*C. carpio*	21.1	0.3	29.4	-6.7	8.3
Jordan barbel	Lake Kinneret	*L. longiceps*	20.1	0.2	29.6	-7.7	9.4
Levantine scraper	Jordan River	*C. damascina*	13.8	0.08			
Jordan himri	Jordan River	*C. canis*	15.7	1.49	24.1	-6.3	8.4
Fossil fish teeth							
UB II-38C#100	UB	*L. longiceps*	19.2		29.2	-3.11	10.0
UB II-38C#101	UB	*L. longiceps*	20.2		28.4	-3.57	8.2
U II-38C#102	UB	*L. longiceps*	20.7		29.1	-3.99	8.5
UB II-38C#103	UB	*L. longiceps*	19.6		28.4	-3.22	8.8
UB II-36Ca-E	UB	*L. longiceps*	20.0				
UB II-23Ca-E	UB	*L. longiceps*	17.4		25.5	-6.39	8.1
UB II-23Ca-E	UB	*L. longiceps*	18.1		25.5		7.4
UB III-2012Ca-E	UB	*L. longiceps*	18.0				
UB III-2012Ca-E	UB	*L. longiceps*	16.9				
GBY 6.2-E	B	*L. longiceps*	15.6				
GBY 6.0-E	B	*L. longiceps*	17.4				
GBY #8622	A	*L. longiceps*	14.1	0.03	26.1	-7.97	12.0
GBY #8697	A	*L. longiceps*	14.1	0.08	25.2	-8.19	11.2
GBY #8696	A	*L. longiceps*	16.1	0.16	24.6	-7.64	8.5
GBY #8714	A	*L. longiceps*	12.9	0.17			
GBY #42098	C V5	*L. longiceps*	15.4	0.04	26.4	-7.31	11.0
GBY #42099	C V5	*L. longiceps*	15.4	0.16	23.7	-7.38	8.3
GBY #60030	II-6 L1	*L. longiceps*	15.4	0.24	23.6	-7.10	8.2
GBY# 60008	II-6 L1	*L. longiceps*	16.4	0.54	24.9	-6.57	8.6
GBY #60737	II-6 L1	*L. longiceps*	15.7	0.12			
GBY #60016	II-6 L1	*L. longiceps*	12.8	0.20	25.4	-6.94	12.6
GBY #1065	II-6 L2	*L. longiceps*	15.6	0.13			
GBY #1175	II-6 L2	*L. longiceps*	15.8	0.13			
GBY #1176	II-6 L2	*L. longiceps*	15.2	0.34			
GBY #1396	II-6 L2	*L. longiceps*	15.7	0.01			

Supplementary Table 6. *cont.*

GBY #63321	II-6 L3	*L. longiceps*	17.2	0.17			
GBY #63129	II-6 L3	*L. longiceps*	17.8	0.12			
GBY# 63116	II-6 L3	*L. longiceps*	16.5	0.01			
GBY #63450	II-6 L3	*L. longiceps*	16.0	0.11	26.5	-7.09	10.6
GBY #63116	II-6 L3	*L. longiceps*	16.2	0.16			
GBY #67029	II-6 L4	*L. longiceps*	15.8	0.43	23.9	-7.32	8.1
GBY #74894	II-6 L5	*L. longiceps*	16.5	0.04	26.1	-6.34	9.6
GBY# 74774	II-6 L5	*L. longiceps*	17.0	0.14			
GBY #80309	II-6 L6	*L. longiceps*	16.3	0.10	25.9	-7.01	9.6
GBY #83289	II-6 L7	*L. longiceps*	15.7	0.09	23.4	-6.68	7.7
GBY 83260	II-6 L7	*L. longiceps*	15.4	0.25			
GBY #83285	II-6 L7	*L. longiceps*	15.3	0.13	23.5	-6.83	8.1
GBY #83261	II-6 L7	*L. longiceps*	14.3	0.07	25.7	-7.40	11.4

GBY = Gesher Benot Ya'aqov, UB = 'Ubeidiya

Supplementary Table 7. Discriminant function analyses posterior probabilities among the various habitats based on the phosphate and the carbonate fraction isotope composition ($\delta^{18}O_{PO4}$-$\delta^{13}C$) in the sampled teeth.

Row	Actual Habitat	SqDist (Actual)	Prob (Actual)	Log (Prob)	Misclassified	Predicted (Pred)	Prob (Pred)	Others
8	UB	1.853	1.000	0.000		UB	1.000	
9	UB	0.648	1.000	0.000		UB	1.000	
10	UB	2.416	1.000	0.000		UB	1.000	
11	UB	0.866	1.000	0.000		UB	1.000	
13	UB	3.442	0.235	1.447	*	GBY B	0.500	JR 0.26
1	Kinneret	-0.307	1.000	0.000		Kinneret	1.000	
2	Kinneret	-0.440	0.999	0.001		Kinneret	0.999	
3	Kinneret	-1.860	1.000	0.000		Kinneret	1.000	
4	Kinneret	-2.149	1.000	0.000		Kinneret	1.000	
5	Kinneret	-0.162	1.000	0.000		Kinneret	1.000	
7	JR	-0.700	0.773	0.258		JR	0.773	GBY B 0.22
21	GBY B	-1.820	0.757	0.278		GBY B	0.757	JR 0.24
22	GBY B	-0.737	0.630	0.463		GBY B	0.630	JR 0.35
24	GBY B	4.198	0.813	0.207		GBY B	0.813	JR 0.19
32	GBY B	-1.350	0.787	0.239		GBY B	0.787	JR 0.20
34	GBY B	-0.033	0.719	0.329		GBY B	0.719	JR 0.26
35	GBY B	1.113	0.368	1.000	*	Jordan River	0.592	
37	GBY B	-1.223	0.804	0.219		GBY B	0.804	JR 0.18

Supplementary Table 7. *cont.*

38	GBY B	-1.551	0.643	0.442		GBY B	0.643	JR 0.35
40	GBY B	-1.961	0.702	0.354		GBY B	0.702	JR 0.30
41	GBY B	0.174	0.674	0.394		GBY B	0.674	JR 0.33
17	GBY A	-2.794	0.962	0.039		GBY A	0.962	
18	GBY A	-2.794	0.981	0.020		GBY A	0.981	
19	GBY A	-2.794	0.953	0.048		GBY A	0.953	

UB = 'Ubeidiya; Kinneret = Lake Kinneret; JR = Jordan River

Supplementary **Table 8.** Tukey HSD pairwise comparison between $\delta^{18}O_{PO4}$ (‰) values identified at Gesher Benot Ya'aqov, by excavated Areas (A *vs.* B), at paleo-Lake 'Ubeidiya (1.5 Mya) and modern-day Lake Kinneret (significant difference marked in red).

Site locality	Site locality	Difference	Std Error	t Ratio	Prob>|t|	Lower 95%	Upper 95%
GBY-A	UB	-5.017	0.618	-8.114	<0.0001	-6.833	-3.201
GBY-B	UB	-3.182	0.445	-7.152	<0.0001	-4.489	-1.876
GBY-A	Modern	-3.548	0.660	-5.372	0.0001	-5.488	-1.608
GBY-B	Modern	-1.713	0.502	-3.414	0.0170	-3.188	-0.239
GBY-A	GBY-B	-1.834	0.573	-3.199	0.0279	-3.519	-0.150
Modern	UB	-1.469	0.553	-2.658	0.0897	-3.092	0.154

REFERENCES CITED:

1 Adán, G. E., Álvarez-Lao, D., Turrero, P., Arbizu, M. & García-Vázquez, E. Fish as diet resource in North Spain during the Upper Paleolithic. *J. Archaeol. Sci.* **36**, 895–899, doi:http://dx.doi.org/10.1016/j.jas.2008.11.017 (2009).

2 Archer, W. & Braun, D. R. Investigating the Signature of Aquatic Resource Use within Pleistocene Hominin Dietary Adaptations. *PLoS ONE* **8**, e69899, doi:https://doi.org/10.1371/journal.pone.0069899 (2013).

3 Braun, D. R. *et al.* Early hominin diet included diverse terrestrial and aquatic animals 1.95 Ma in East Turkana, Kenya. *Proc. Natl. Acad. Sci.* **107**, 10002–10007, doi:https://doi.org/10.1073/pnas.1002181107 (2010).

4 Stewart, K. M. Early hominid utilisation of fish resources and implications for seasonality and behaviour. *J. Hum. Evol.* **27**, 229–245 (1994).

5 Joordens, J. C. A., Wesselingh, F. P., de Vos, J., Vonhof, H. B. & Kroon, D. Relevance of aquatic environments for hominins: A case study from Trinil (Java, Indonesia). *J. Hum. Evol.* **57**, 656–671, doi:https://doi.org/10.1016/j.jhevol.2009.06.003 (2009).

6 Bar-Yosef, O. Prehistory of the Levant. *Ann. Rev. Anthropol.* **9**, 101–133 (1980).

7 Bar-Yosef, O. & Goren-Inbar, N. *The lithic assemblages of 'Ubeidiya*. Vol. 34, 1–266 (Hebrew University of Jerusalem, 1993).

8 Stewart, K. M. *Fishing sites of North and East Africa in the Late Pleistocene and Holocene*. Vol. 521, 1–274 (B.A.R. 521, 1989).

9 Goren-Inbar, N., Alperson-Afil, N., Sharon, G. & Herzlinger, G. *The Acheulian site of Gesher Benot Ya'aqov* Vol. Volume IV, 1–461 (Springer International Publishing, 2018).

10 Goren-Inbar, N. *et al.* Pleistocene milestones on the out-of-Africa corridor at Gesher Benot Ya'aqov. *Science* **289**, 944–947 (2000).

11 Feibel, C. S. in *Human Paleoecology in the Levantine Corridor* (eds N. Goren-Inbar & J.D. Speth) Ch. 2, 21–36 (Oxbow Books, 2004).

12 Feibel, C. S. in *Sediments in Archaeological Context* (eds J.K. Stein & W.R. Farrand) 127–148 (The University of Utah Press, 2001).

13 Berger, A. *et al.* Interglacials of the last 800,000 years. *Rev.Geophys.* **54**, 162–219, doi:https://doi.org/10.1002/2015RG000482 (2016).

14 Goren-Inbar, N. *et al.* New discoveries at the Middle Pleistocene Acheulian site of Gesher Benot Ya'aqov, Israel. *Quat. Res.* **38**, 117–128 (1992).

15 Goren-Inbar, N. Culture and cognition in the Acheulian industry: A case study from Gesher Benot Ya'aqov. *Philos. Trans. R. Soc. Lond., B, Biol. Sci.* **366**, 1038–1049, doi:10.1098/rstb.2010.0365 (2011).

16 Goren-Inbar, N. *et al.* Evidence of hominid control of fire at Gesher Benot Ya'aqov, Israel. *Science* **304**, 725–726, doi:10.1126/science.1095443 (2004).

17 Goren-Inbar, N. & Belfer-Cohen, A. in *Neandertals and Modern Humans in Western Asia* (eds T. Akazawa, K. Aoki, & B. Bar-Yosef) 205–221 (Plenum Press, 1998).

18 Goren-Inbar, N., Melamed, Y., Zohar, I., Akhilesh, K. & Pappu, S. Beneath still waters - Multistage aquatic exploitation of *Euryale ferox* (Salisb.) during the Acheulian. *Internet Archaeol.* **37**, 1–42, doi:10.11141/ia.37.1 (2014).

19 Melamed, Y., Kislev, M., Weiss, E. & Simchoni, O. Extinction of water plants in the Hula Valley: Evidence for climate change. *J. Hum. Evol.* **60**, 320–327, doi:https://doi.org/10.1016/j.jhevol.2010.07.025 (2011).

20 Rabinovich, R., Gaudzinski-Windheuser, S. & Goren-Inbar, N. Systematic butchering of fallow deer (*Dama*) at the early middle Pleistocene Acheulian site of Gesher Benot Ya'aqov (Israel). *J. Hum. Evol.* **54**, 134–149, doi:10.1016/j.jhevol.2007.07.007 (2008).

21 Rabinovich, R., Gaudzinski-Windheuser, S., Kindler, L. & Goren Inbar, N. *The Acheulian site of Gesher Benot Ya'aqov: Mammalian Taphonomy, The Assemblages of Layers V-5 and V-6*. Vol. 3, 1–269 (Springer, 2012).

22 Saragusti, I. & Goren-Inbar, N. The biface assemblage from Gesher Benot Ya'aqov, Israel: illuminating patterns in "Out of Africa" dispersal. *Quat. Int.* **75**, 85–89, doi:https://doi.org/10.1016/S1040-6182(00)00080-X (2001).

23 Mienis, H. K. & Ashkenazi, S. Lentic Basommatophora molluscs and hygrophilous land snails as indicators of habitat and climate in the Early-Middle Pleistocene (0.78 Mya) at the site of Gesher Benot Ya'aqov (GBY), Israel. *J. Hum. Evol.* **60**, 328–340, doi:10.1016/j.jhevol.2010.03.009 (2011).

24 Spiro, B., Ashkenazi, S., Starinsky, A. & Katz, A. Strontium isotopes in *Melanopsis* sp. as indicators of variation in hydrology and climate in the Upper Jordan Valley during the Early–Middle Pleistocene, and wider implications. *J. Hum. Evol.* **60**, 407–416, doi:http://dx.doi.org/10.1016/j.jhevol.2010.07.026 (2011).

25 Van Zeist, W. & Bottema, S. A palynological study of the Acheulian site of Gesher Benot Ya'aqov, Israel. *Veget. Hist. Archaeobot.* **18**, 105–121, doi:10.1007/s00334-008-0167-5 (2008).

26 Alperson-Afil, N. *et al.* Spatial organization of hominin activities at Gesher Benot Ya'aqov, Israel. *Science* **326**, 1677–1680, doi:10.11rob26/science.1180695 (2009).

27 Zohar, I. & Biton, R. Land, lake, and fish: Investigation of fish remains from Gesher Benot Ya'aqov (paleo-Lake Hula). *J. Hum. Evol.* **60**, 343–356, doi:https://doi.org/10.1016/j.jhevol.2010.10.007 (2011).

28 Melamed, Y., Kislev, M. E., Geffen, E., Lev-Yadun, S. & Goren-Inbar, N. The plant component of an Acheulian diet at Gesher Benot Ya'aqov, Israel. *Proc. Natl. Acad. Sci.* **113**, 14674–14679, doi: https://doi.org/10.1073/pnas.1607872113 (2016).

29 Ashkenazi, S., Motro, U., Goren-Inbar, N., Biton, R. & Rabinovich, R. New morphometric parameters for assessment of body size in the fossil freshwater crab assemblage from the Acheulian site of Gesher Benot Ya'aqov, Israel. *J. Archaeol. Sci.* **32**, 675–689, doi:http://dx.doi.org/10.1016/j.jas.2004.12.003 (2005).

30 Rabinovich, R. & Biton, R. The Early–Middle Pleistocene faunal assemblages of Gesher Benot Ya'aqov: Inter-site variability. *J. Hum. Evol.* **60**, 357–374, doi:10.1016/j.jhevol.2010.12.002 (2011).

31 Goren-Inbar, N., Lister, A., Werker, E. & Chech, M. A butchered elephant skull and associated artifacts from the Acheulian site of Gesher Benot Ya'Aqov, Israel. *Paléorient* **20**, 99–112 (1994).

32 Werker, E. 780,000-Year-old wood from Gesher Benot Ya'aqov, Israel. *Israel J. Plant Sci.* **54**, 291–300 (2007).

33 Herzlinger, G. & Goren-Inbar, N. Do a few tools necessarily mean a few people? A techno-morphological approach to the question of group size at Gesher Benot Ya'aqov, Israel. *J. Hum. Evol.* **128**, 45–58, doi:https://doi.org/10.1016/j.jhevol.2018.11.008 (2019).

34 Goren-Inbar, N. & Belfer-Cohen, A. Reappraisal of hominin group size in the Lower Paleolithic: An introduction to the special issue. *J. Hum. Evol.* **144**, 102821, doi:10.1016/j.jhevol.2020.102821 (2020).

35 Alperson-Afil, N. Continual fire-making by Hominins at Gesher Benot Ya'aqov, Israel. *Quat. Sci. Rev.* **27**, 1733–1739, doi:10.1016/j.quascirev.2008.06.009 (2008).

36 Alperson-Afil, N. Archaeology of fire: Methodological aspects of reconstructing fire history of prehistoric archaeological sites. *Earth Sci. Rev.* **113**, 111–119, doi:10.1016/j.earscirev.2012.03.012 (2012).

37 Alperson-Afil, N. & Goren-Inbar, N. *The Acheulian site of Gesher Benot Ya'aqov: Ancient flames and controlled use of fire*. Vol. Volume II, (Springer, 2010).

38 Alperson-Afil, N., Richter, D. & Goren-Inbar, N. Phantom hearths and the use of fire at Gesher Benot Ya'aqov, Israel. *PaleoAnthropology* **1**, 1–15 (2007).

39 Alperson-Afil, N., Richter, D. & Goren-Inbar, N. Evaluating the intensity of fire at the Acheulian site of Gesher Benot Ya'aqov—Spatial and thermoluminescence analyses. *PLoS ONE* **12**, e0188091, doi: https://doi.org/10.1371/journal.pone.0188091 (2017).

40 Goren, M. & Ortal, R. Biogeography, diversity and conservation of the inland water fish communities in Israel. *Biol. Cons.* **89**, 1–9 (1999).

41 Banarescu, P. & Coad, B. W. in *Cyprinid Fishes: Systematic, ecology and exploitation* Vol. Series 3 *Fish and Fisheries* (eds I.J. Winfield & J.S. Nelson) 127–155 (Chapman & Hall, 1991).

42 Berra, T. M. *Freshwater Fish Distribution*. (Academic Press, 2001).

43 Durand, J. D., Tsigenopoulos, C. S., Unlü, E. & Berrebi, P. Phylogeny and biogeography of the family Cyprinidae in the Middle East inferred from cytochrome *b* DNA- evolutionary significance of this region *Mol. Phylogenet. Evol.* **22**, 91–100, doi:doi: 10.1006/mpev.2001.1040. (2002).

44 Goren, M., Fishelson, L. & Trewavas, E. The Cyprinid fishes of *Acanthobrama* Heckel and related genera. *Bull. Br. Mus. nat, Hist. (zool.)* **24**, 293–315 (1973).

45 Por, D. F. & Dimentman, C. *Mare Nostrum: Neogene and anthropic natural history of the Mediterranean Basin, with emphasis on the Levant*. (Pensoft Publishers, 2006).

46 Por, F. D. *The Legacy of Tethys: An Aquatic Biogeography of the Levant*. Vol. Vol. 63, (Kluwer Academic Publisher, 1989).

47 Goren, M. The freshwater fishes of Israel. *Isr. J. Zool.* **23**, 67–118 (1974).

48 Krupp, F. & Schneider, W. The fishes of the Jordan River drainage basin and Azraq Oasis. *Fauna of Saudi Arabia* **10**, 348–415 (1989).

49 Dimentman, C., Bromley, H. J. & Por, D. F. *Lake Hula: Reconstruction of the fauna and hydrobiology of a lost lake*. (The Israel Academy of Sciences and Humanities, 1992).

50 Simopoulos, A. Omega-3 fatty acids in health and disease and in growth and development. *Am. J. Clin. Nutr.* **54**, 438–463, doi:10.1093/ajcn/54.4.771 (1991).

51 Hantoush, A. A., Al-Hamadany, Q. H., Al-Hassoon, A. S. & Al-Ibadi, H. Nutritional value of important commercial fish from Iraqi waters. *Int. J. Mar. Sci.* **5**, 13–22 (2015).

52 Ljubojević, D. *et al.* Fatty acid composition of fishes from Inland Waters. *Bulg. J. Agric. Sci.* **19**, 62–71 (2013).

53 Kawarazuka, N. & Béné, C. Linking small-scale fisheries and aquaculture to household nutritional security: An overview. *Food Sec.* **2**, 343–357, doi:10.1007/s12571-010-0079-y (2010).

54 Nakajima, T. & Yue, P. Q. Morphological changes in development of pharyngeal teeth in *Mylopharyngodon piceus*. *Chin. J. Oceanol. Limnol.* **13**, 271–277 (1995).

55 Pasco-Viel, E. *et al.* Evolutionary trends of the pharyngeal dentition in Cypriniformes (Actinopterygii: Ostariophysi). *PLoS ONE* **5**, e11293, doi:10.1371/journal.pone.0011293 (2010).

56 Nakajima, T. Larval *vs*. adult pharyngeal dentition in some Japanese cyprinid fishes. *J. Dent. Res.* **63**, 1140–1146, doi:10.1177/00220345840630090901 (1984).

57 Zohar, I., Goren, M. & Goren-Inbar, N. Fish and ancient lakes in the Dead Sea Rift: The use of fish remains to reconstruct the ichthyofauna of paleo-Lake Hula. *Palaeogeogr. Palaeoclimatol. Palaeoecol.* **405**, 28–41, doi:http://dx.doi.org/10.1016/j.palaeo.2014.04.006 (2014).

58 Banister, K. E. A revision of the large *Barbus* (Pisces, Cyprinidae) of East and Central Africa. Studies on African Cyprinidae Part II. *Bull. Br. Mus. Nat. Hist.* **26**, 1–148 (1973).

59 Böhme, M. Revision of the cyprinids from the Early Oligocene of the České Středohoří mountains, and the phylogenetic relationships of *Protothymallus laube* 1901 (Teleostei, Cyprinidae, Gobioninae). *Acta Mus. Nat. Pragae, Ser. B Hist. Nat.* **63**, 175–194 (2007).

60 Zohar, I. *Fish exploitation at the Sea of Galilee (Israel) by early fisher-hunter-gatherers (23,000 B.P.): Ecological, economical, and cultural Implications* PhD thesis, Tel Aviv University, (2003).

61 Gibert, Y. *et al. Altered retinoic acid signalling underpins dentition evolution*. Vol. 282, (2015).

62 Debiais-Thibaud, M. *et al.* Development of oral and pharyngeal teeth in the Medaka (*Oryzias latipes*): Comparison of morphology and expression of eve1 gene. *J. Exp. Zool. Part B* **308**, 693–708, doi:10.1002/jez.b.21183 (2007).

63 Mullaney, M. D. & Gale, L. D. Ecomorphological relationships in ontogeny: Anatomy and diet in Gag, *Mycteroperca microlepis* (Pisces: Serranidae). *Copeia* **1996**, 167–180, doi:10.2307/1446952 (1996).

64 Rosa, J. T., Witten, P. E. & Huysseune, A. Cells at the Edge: The dentin–bone interface in Zebrafish teeth. *Front. Physiol.* **12**, doi:10.3389/fphys.2021.723210 (2021).

65 Fink, W. L. Ontogeny and phylogeny of tooth attachment modes in actinopterygian fishes. *J. Morphol.* **167**, 167–184 (1981).

66 Witten, P. E. & Huysseune, A. A comparative view on mechanisms and functions of skeletal remodelling in teleost fish, with special emphasis on osteoclasts and their function. *Biol. Rev.* **84**, 315–346, doi:https://doi.org/10.1111/j.1469-185X.2009.00077.x (2009).

67 Huysseune, A., Sire, J.-Y. & Witten, P. E. Evolutionary and developmental origins of the vertebrate dentition. **214**, 465–476, doi:https://doi.org/10.1111/j.1469-7580.2009.01053.x (2009).

68 Nakajima, T., Yoshida, H., Hotta, Y. & Sone, B. Tooth replacements in the crucian carps, the genus *Carassins* of the family Cyprinidae. *Jpn. J. Oral Biol.* **28**, 370–374, doi:https://doi.org/10.2330/joralbiosci1965.28.370 (1986).

69 Van den Brink, E. C. M. *et al.* Late Chalcolithic settlement remains East of Namir Road. *JIPS* **46**, 20–121 (2016).

70 Van der Heyden, C., Huysseune, A. & Sire, J. Y. Development and fine structure of pharyngeal replacement teeth in juvenile zebrafish (*Danio rerio*) (Teleostei, Cyprinidae). *Cell Tissue Res.* **302**, 205–219, doi:10.1007/s004410000180 (2000).

71 Borday-Birraux, V. *et al.* Expression of Dlx genes during the development of the zebrafish pharyngeal dentition: evolutionary implications. *Evol. Dev.* **8**, 130–141, doi:10.1111/j.1525-142X.2006.00084.x (2006).

72 Huysseune, A., Sire, J.-Y. & Meunier, F. J. Comparative study of lower pharyngeal jaw structure in two phenotypes of *Astatoreochromis alluaudi* (Teleostei: Cichlidae). **221**, 25–43 (1994).

73 Hughes, D., Bassett, J. & Moffat, L. Structure and origin of the tooth pedicel (the so-called bone of attachment) and dental-ridge bone in the mandibles of the sea breams *Acanthopagrus australis, Pagrus auratus* and *Rhabdosargus sarba* (Sparidae, Perciformes, Teleostei). *J. Anat. Embryol.* **189**, 51–69, doi:10.1007/BF00193129 (1994).

74 Nemoto, Y., Higuchi, K., Baba, O., Kudo, A. & Takano, Y. Multinucleate osteoclasts in medaka as evidence of active bone remodeling. *Bone* **40**, 399–408, doi:https://doi.org/10.1016/j.bone.2006.08.019 (2007).

75 Abduweli, D. *et al.* Tooth replacement and putative odontogenic stem cell niches in pharyngeal dentition of medaka (*Oryzias latipes*). *Microscopy* **63**, 141–153, doi:10.1093/jmicro/dft085 (2014).

76 Zohar, I., Ovadia, A. & Goren-Inbar, N. The cooked and the raw: A taphonomic study of cooked and burned fish. *J. Archaeol. Sci. Rep.* **8**, 164–172, doi:http://dx.doi.org/10.1016/j.jasrep.2016.06.005 (2016).

77 Behrensmeyer, A. K. in *Animals and Archaeology: 1. Hunters and Their Prey* Vol. 163 (eds J. Clutton-Brock & C. Grigson) 93–106 (British Archaeological Reports International Series, 1983).

78 Butler, V. L. in *Natural Formation Process and the Archaeological Record* Vol. 352 (eds D.T. Nash & M.D. Petraglia) 131–149 (B.A.R. 352, 1987).

79 Butler, V. L. *Distinguishing natural from cultural Salmonid deposits in the Pacific Northwest of North America*, University of Washington, (1990).

80 Butler, V. L. Natural versus cultural Salmonid remains: Origin of the Dalles Roadcut bones, Columbia River, Oregon, USA. *J. Archaeol. Sci.* **20**, 1–24, doi:https://doi.org/10.1006/jasc.1993.1001 (1993).

81 Stewart, K. M. Modern fishbone assemblages at Lake Turkana, Kenya: A methodology to aid in recognition of Hominid fish utilization. *J. Archaeol. Sci.* **18**, 579–603 (1991).

82 Stewart, K. M. & Gifford-Gonzales, D. An ethnoarchaeological contribution to identifying hominid fish processing sites. *J. Archaeol. Sci.* **21**, 237–248 (1994).

83 Zohar, I. *et al.* The living and the dead: How do taphonomic processes modify relative abundance and skeletal completeness of freshwater fish? *Palaeogeogr. Palaeoclimatol. Palaeoecol.* **258**, 292–316, doi:https://doi.org/10.1016/j.palaeo.2007.11.004 (2008).

84 Gifford-Gonzalez, D., Stewart, M. K. & Rybczynski, N. Human activities and site formation at modern lake margin foraging camps in Kenya. *J. Anthropol. Archaeol.* **18**, 397–440, doi:https://doi.org/10.1006/jaar.1999.0337 (1999).

85 Zohar, I. & Cooke, R. The role of dried fish: A taphonomical model of fish butchering and long-term preservation. *J. Archaeol. Sci. Rep.* **26**, 101864, doi:https://doi.org/10.1016/j.jasrep.2019.05.029 (2019).

86 Zohar, I., Dayan, T., Goren, M., Nadel, D. & Hershkovitz, I. Opportunism or aquatic specialization? Evidence of freshwater fish exploitation at Ohalo II–a waterlogged Upper Paleolithic site. *PLoS ONE* **13**, 1–28 (2018).

87 Guillaud, E., Bearez, P., Denys, C. & Raimond, S. New data on fish diet and bone digestion of the Eurasian otter (*Lutra lutra*) (Mammalia: Mustelidae) in central France. *Eur. Zool. J.* **84**, 226–237, doi:10.1080/24750263.2017.1315184 (2017).

88 Wilson, M. V. H. Predation as a source of fish fossils in Eocene lake sediments. *Palaios* **2**, 497–504, doi:10.2307/3514620 (1987).

89 Elder, R. L. & Smith, G. R. Fish taphonomy and environmental inference in paleolimnology. *Palaeogeogr. Palaeoclimatol. Palaeoecol.* **62**, 577–592 (1988).

90 Ferber, C. T. & Wells, N. A. Paleolimnology and taphonomy of some fish deposits in "Fossil" and "Uinta" lakes of the Eocene Green River Formation, Utah and Wyoming. *Palaeogeogr. Palaeoclimatol. Palaeoecol.* **117**, 185–210 (1995).

91 Agiadi, K. & Albano, P. G. Holocene fish assemblages provide baseline data for the rapidly changing eastern Mediterranean. *Holocene* **30**, 1438–1450, doi:10.1177/0959683620932969 (2020).

92 Lin, C.-H. *et al.* Reconstructing reef fish communities using fish otoliths in coral reef sediments. *PLoS ONE* **14**, e0218413, doi:10.1371/journal.pone.0218413 (2019).

93 Sibert, E., Cramer, K., Hastings, P. & Norris, R. D. Methods for isolation and quantification of microfossil fish teeth and elasmobranch dermal denticles (Ichthyoliths) from marine sediments. *Palaeontol. Electron.* **20**, doi:10.26879/677 (2017).

94 Collins, S. E. & Underwood, C. J. Unique damage-related, gap-filling tooth replacement in pycnodont fishes. *Palaeontology* **64**, 489–504, doi:https://doi.org/10.1111/pala.12539 (2021).

95 Analytic Rarefaction v. V.1.3 (http://strata.uga.edu/software/anRareReadme.html, University of Georgia, Stratigraphic Lab., 2001).

96 Shimosaka, C., Shimomura, M. & Terai, M. Changes in the physical properties and composition of fish bone during cooking by heating under normal pressure. *J. Home Econ. Jpn.* **47**, 1213–1218 (1996).

97 Richter, J. Experimental study of heat-induced morphological changes in fish bone collagen. *J. Archaeol. Sci.* **13**, 477–481, doi:10.1016/0305-4403(86)90017-8 (1986).

98 Ishikawa, M., Mori, S., Watanabe, H. & Sakai, Y. Softening of fish bone. II. Effect of acetic acid on softening rate and solubilization rate of organic matter from fish bone. *J. Food Process. Preserv.* **13**, 123–132, doi:10.1111/j.1745-4549.1989.tb00095.x (1989).

99 Bastías, J. M., Balladares, P., Acuña, S., Quevedo, R. & Muñoz, O. Determining the effect of different cooking methods on the nutritional composition of salmon (*Salmo salar*) and Chilean jack mackerel (*Trachurus murphyi*) fillets. *PLoS ONE* **12**, e0180993-e0180993, doi:10.1371/journal.pone.0180993 (2017).

100 Luebke, A. *et al.* Reply to the 'Comments on "Dental lessons from past to present: ultrastructure and composition of teeth from plesiosaurs, dinosaurs, extinct and recent sharks"' by H. Botella et al., RSC Adv., 2016, 6, 74384–74388. *RSC Advances* **7**, 6215–6222, doi:10.1039/C6RA27121A (2017).

101 Deang, J. F. *et al.* Structure, property, and function of sheepshead (Archosargus probatocephalus) teeth. *Arch. Oral Biol.* **89**, 1–8, doi:https://doi.org/10.1016/j.archoralbio.2018.01.013 (2018).

102 Kawasaki, K. *et al.* Coevolution of enamel, ganoin, enameloid, and their matrix SCPP genes in osteichthyans. *Science* **24**, 102023–102023, doi:10.1016/j.isci.2020.102023 (2021).

103 LeGeros, R. Z. Properties of osteoconductive biomaterials: Calcium Phosphates. *Clin. Orthop. Relat. Res.* **395**, 81–98 (2002).

104 LeGeros, R. Z. Apatites in biological systems. *Prog. Cryst. Growth Charact. Mater.* **4**, 1–45, doi:https://doi.org/10.1016/0146-3535(81)90046-0 (1981).

105 LeGeros, R. Z., Trautz, O. R., Legeros, J. P., Klein, E. & Shirra, W. P. Apatite crystallites: Effects of carbonate on morphology. *Science* **155**, 1409–1411, doi:10.1126/science.155.3768.1409 (1967).

106 Reyes-Gasga, J., MartÍnez-Piñeiro, E. L. & Brés, É. F. Crystallographic structure of human tooth enamel by electron microscopy and x-ray diffraction: hexagonal or monoclinic? *J. Microsc.* **248**, 102–109, doi:10.1111/j.1365-2818.2012.03653.x (2012).

107 Fleet, M. *Carbonated Hydroxyapatite: Materials, Synthesis, and Applications*. 1–278 (Pan Stanford Publishing, 2014).

108 Shemesh, A. Crystallinity and diagenesis of sedimentary apatites. *Geochim. Cosmochim. Acta.* **54**, 2433–2438, doi:https://doi.org/10.1016/0016-7037(90)90230-I (1990).

109 Lopes, C. d. C. A., Limirio, P. H. J. O., Novais, V. R. & Dechichi, P. Fourier transform infrared spectroscopy (FTIR) application chemical characterization of enamel, dentin and bone. *Appl. Spectrosc. Rev.* **53**, 1–23, doi:https://doi.org/10.1080/05704928.2018.1431923 (2018).

110 Hanlie, H., Liyun, T. & Tao, J. The crystal characteristics of enamel and dentin by XRD method. *J. Wuhan Univ. Technol.-Mat. Sci. Edit.* **21**, 9, doi:10.1007/BF02861458 (2006).

111 Zhuang, Z., Yoshimura, H. & Aizawa, M. Synthesis and ultrastructure of plate-like apatite single crystals as a model for tooth enamel. *Mater. Sci. Eng. C* **33**, 2534–2540, doi:https://doi.org/10.1016/j.msec.2013.02.035 (2013).

112 Miake, Y. *et al.* Ultrastructural studies on crystal growth of enameloid minerals in elasmobranch and teleost fish. *Calcif. Tissue Int.* **48**, 204–217, doi:10.1007/BF02570556 (1991).

113 Kallaste, T. & Nemliher, J. Apatite varieties in extant and fossil vertebrate mineralized tissues. *J. Appl. Crystallogr.* **38**, 587–594 (2005).

114 Kallaste, T. & Nemliher, J. Conodont bioapatite resembles vertebrate enamel by XRD properties. *EST. J. EARTH SCI.* **61**, 191–192, doi:10.3176/earth.2012.3.05 (2012).

115 Becker, M. A., Seidemann, D. E., Chamberlain, J. A., Buhl, D. & Slattery, W. Strontium isotopic signatures in the enameloid and dentine of upper Cretaceous shark teeth from western Alabama: Paleoecologic and geochronologic implications. *Palaeogeogr. Palaeoclimatol. Palaeoecol.* **264**, 188–194, doi:https://doi.org/10.1016/j.palaeo.2008.04.006 (2008).

116 Tütken, T. *et al.* Strontium and oxygen isotope analyses reveal Late Cretaceous shark teeth in Iron Age strata in the Southern Levant. *Front. Ecol. Evol.* **8**, doi:https://doi.org/10.3389/fevo.2020.570032 (2020).

117 Madupalli, H., Pavan, B. & Tecklenburg, M. M. J. Carbonate substitution in the mineral component of bone: Discriminating the structural changes, simultaneously imposed by carbonate in A and B sites of apatite. *J. Solid State Chem.* **255**, 27–35, doi:10.1016/j.jssc.2017.07.025 (2017).

118 Koch, P. L., Tuross, N. & Fogel, M. L. The effects of sample treatment and diagenesis on the isotopic integrity of carbonate in biogenic hydroxylapatite. *J. Archaeol. Sci.* **24**, 417–429, doi:https://doi.org/10.1006/jasc.1996.0126 (1997).

119 Reiche, I., Vignaud, C. & Menu, M. The crystallinity of ancient bone and dentine: new insights by transmission electron microscopy. *Archaeometry* **44**, 447–459, doi:10.1111/1475-4754.00077 (2002).

120 Pollard, A., Batt, C. M., Stern, B. & Young, S. M. M. *Analytical Chemistry in Archaeology*. (Cambridge University Press, 2007).

121 Białas, N. *et al.* Teeth of past and present elephants: Microstructure and composition of enamel in fossilized proboscidean molars and implications for diagenesis. *Geochem, Geophys. Geosys.* **22**, e2020GC009557, doi:https://doi.org/10.1029/2020GC009557 (2021).

122 Piga, G. *et al.* A structural approach in the study of bones: fossil and burnt bones at nanosize scale. *Appl. Phys. A* **122**, 1031, doi:10.1007/s00339-016-0562-1 (2016).

123 Piga, G. *et al.* Understanding the crystallinity indices behavior of burned bones and teeth by ATR-IR and XRD in the presence of bioapatite mixed with other phosphate and carbonate phases. *Int. J. Spectrosc.* **2016**, 1–9, doi:https://doi.org/10.1155/2016/4810149 (2016).

124 Piga, G., Malgosa, A., Thompson, T. & Enzo, S. A new calibration of the XRD technique for the study of archaeological burned human remains. *J. Archaeol. Sci.* **35**, 2171–2178 (2008).

125 Piga, G. *et al.* A multi-technique approach by XRD, XRF, FT-IR to characterize the diagenesis of dinosaur bones from Spain. *Palaeogeogr. Palaeoclimatol. Palaeoecol.* **310**, 92–107, doi:https://doi.org/10.1016/j.palaeo.2011.05.018 (2011).

126 Thompson, T. J. U., Islam, M. & Bonniere, M. A new statistical approach for determining the crystallinity of heat-altered bone mineral from FTIR spectra. *J. Archaeol. Sci.* **40**, 416–422, doi:http://dx.doi.org/10.1016/j.jas.2012.07.008 (2013).

127 Piga, G., Thompson, T. J. U., Malgosa, A. & Enzo, S. The potential of X-ray diffraction in the analysis of burned remains from forensic contexts. *J. Forensic Sci.* **54**, 534–539, doi:https://doi.org/10.1111/j.1556-4029.2009.01037.x (2009).

128 Hughes, J. M., Cameron, M. & Crowley, K. D. Structural variations in natural F, OH, and CL apatites. *Am. Mineral* **74**, 870–876 (1989).

129 Schroeder, L. W., Dickens, B. & Brown, W. E. Crystallographic studies of the role of Mg as a stabilizing impurity in β-$Ca_3(PO_4)_2$. II. Refinement of Mg-containing β-$Ca_3(PO_4)_2$. *J. Solid State Chem.* **22**, 253–262, doi:https://doi.org/10.1016/0022-4596(77)90002-0 (1977).

130 Nemliher, J. & Kallaste, T. Thermal behaviour of bone apatite of recent Pike (*Esox lucius* L). *P. EST. ACAD. SCI.* **54**, 112–118 (2005).

131 Nemliher, J. G., Baturin, G. N., Kallaste, T. E. & Murdmaa, I. O. Transformation of hydroxyapatite of bone phosphate from the ocean bottom during fossilization. *LITHOL. MINER. RESOUR.* **39**, 468–479, doi:10.1023/B:LIMI.0000040736.62014.2d (2004).

132 LeGeros, R. Z. Calcium phosphates in oral biology and medicine. *Monogr. Oral Sci.* **15**, 1–201 (1991).

133 Goren-Inbar, N., Sharon, G., Melamed, Y. & Kislev, M. Nuts, nut cracking, and pitted stones at Gesher Benot Ya'aqov, Israel. *Proc. Natl. Acad. Sci.* **99**, 2455–2460, doi:https://doi.org/10.1073/pnas.032570499 (2002).

134 Gilead, I. in *Virtual Archaeology. Proceedings of the VAST Euroconference, Arezzo 24-25 November 2000* Vol. 1075 (ed F. Niccolucci) 41–43 (BAR International Series, 2002).

135 Silverman, B. W. *Density estimation for statistics and data analysis*. (Chapman and Hall, 1986).

136 Kolodny, Y., Luz, B. & Navon, O. Oxygen isotope variations in phosphate of biogenic apatites, I. Fish bone apatite—rechecking the rules of the game. *Earth Planet. Sci. Lett.* **64**, 398–404, doi:http://dx.doi.org/10.1016/0012-821X(83)90100-0 (1983).

137 Longinelli, A. & Nuti, S. Revised phosphate-water isotopic temperature scale. *Earth Planet. Sci. Lett.* **19**, 373–376, doi:https://doi.org/10.1016/0012-821X(73)90088-5 (1973).

138 Lécuyer, C., Amiot, R., Touzeau, A. & Trotter, J. Calibration of the phosphate $\delta^{18}O$ thermometer with carbonate–water oxygen isotope fractionation equations. *Chem. Geol.* **347**, 217–226, doi:http://dx.doi.org/10.1016/j.chemgeo.2013.03.008 (2013).

139 Pucéat, E. *et al.* Revised phosphate–water fractionation equation reassessing paleotemperatures derived from biogenic apatite. *Earth Planet. Sci. Lett.* **298**, 135–142, doi:https://doi.org/10.1016/j.epsl.2010.07.034 (2010).

140 Barrett, J. H. *et al.* Interpreting the expansion of sea fishing in medieval Europe using stable isotope analysis of archaeological cod bones. *J. Archaeol. Sci.* **38**, 1516–1524, doi:10.1016/j.jas.2011.02.017 (2011).

141 Dufour, E. *et al.* Oxygen and strontium isotopes as provenance indicators of fish at archaeological sites: the case study of Sagalassos, SW Turkey. *J. Archaeol. Sci.* **34**, 1226–1239, doi:https://doi.org/10.1016/j.jas.2006.10.014 (2007).

142 Kolodny, Y. & Raab, M. Oxygen isotopes in phosphatic fish remains from Israel: Paleothermometry of tropical Cretaceous and Tertiary shelf waters. *Palaeogeogr. Palaeoclimatol. Palaeoecol.* **64**, 59–67, doi:10.1016/0031-0182(88)90142-3 (1988).

143 Schmitz, B., Åberg, G., Werdelin, L., Forey, P. & Bendix-Almgreen, S. E. $^{87}Sr/^{86}Sr$, Na, F, Sr, and La in skeletal fish debris as a measure of the paleosalinity of fossil-fish habitats. *GSA Bulletin* **103**, 786–794 (1991).

144 Sisma-Ventura, G. *et al.* Past aquatic environments in the Levant inferred from stable isotope compositions of carbonate and phosphate in fish teeth. *PLoS ONE* **14**, e0220390, doi:10.1371/journal.pone.0220390 (2019).

145 Sisma-Ventura, G. *et al.* Tooth oxygen isotopes reveal Late Bronze Age origin of Mediterranean fish aquaculture and trade. *Sci. Rep.* **8**, 14086–14097, doi:10.1038/s41598-018-32468-1 (2018).

146 Sisma-Ventura, G. *et al.* Oxygen isotope composition of Sparidae (Sea bream) tooth enamel from well-dated archaeological sites as an environmental proxy in the East Mediterranean: A case study from Tel Dor, Israel. *J. Archaeol. Sci.* **64**, 46–53, doi:http://dx.doi.org/10.1016/j.jas.2015.10.004 (2015).

147 Roberts, N. *et al.* Stable isotope records of Late Quaternary climate and hydrology from Mediterranean lakes: the ISOMED synthesis. *Quat. Sci. Rev.* **27**, 2426–2441, doi:https://doi.org/10.1016/j.quascirev.2008.09.005 (2008).

148 Gat, J. R. in *Physics and Chemistry of Lakes* (eds A. Lerman, D.M. Imboden, & J.R. Gat) Ch. 5, 139–165 (Springer, 1995).

149 Gat, J. R., Bowser, C. J. & Kendall, C. The contribution of evaporation from the Great Lakes to the continental atmosphere: estimate based on stable isotope data. *Geophys. Res. Lett.* **21**, 557–560, doi:https://doi.org/10.1029/94GL00069 (1994).

150 Stiller, M. & Hutchinson, G. E. The waters of Merom : A study of Lake Huleh. VI. Stable isotopic composition of carbonates of a 54 m core; paleoclimatic and paleotrophic implications. *Arch. Hydrobiol.* **89**, 275–302 (1980).

151 Stiller, M., Ehrlich, A., Pollinger, U., Baruch, U. & Kaufman, A. The late Holocene sediments of Lake Kinneret (Israel)- A multidisciplinary study of a five meter core. *Geol. Surv. Isr. Curr. Res.* **84**, 83–88 (1983-84).

152 Stiller, M. & Magaritz, M. Carbon-13 enriched carbonate in interstitial waters of Lake Kinneret sediments. *Limnol. Oceanogr.* **19**, 849–853 (1974).

153 Kolodny, Y., Luz, B., Sander, M. & Clemens, W. A. Dinosaur bones: fossils or pseudomorphs? The pitfalls of physiology reconstruction from apatitic fossils. *Palaeogeogr. Palaeoclimatol. Palaeoecol.* **126**, 161–171, doi:https://doi.org/10.1016/S0031-0182(96)00112-5 (1996).

154 Martin, C., Bentaleb, I., Kaandorp, R., Iacumin, P. & Chatri, K. Intra-tooth study of modern rhinoceros enamel $\delta^{18}O$: Is the difference between phosphate and carbonate $\delta^{18}O$ a sound diagenetic test? *Palaeogeogr. Palaeoclimatol. Palaeoecol.* **266**, 183–189, doi:https://doi.org/10.1016/j.palaeo.2008.03.039 (2008).

155 Lee-Thorp, J. A., Sealy, J. C. & van der Merwe, N. J. Stable carbon isotope ratio differences between bone collagen and bone apatite, and their relationship to diet. *J. Archaeol. Sci.* **16**, 585–599, doi:https://doi.org/10.1016/0305-4403(89)90024-1 (1989).

156 Pellegrini, M., Lee-Thorp, J. A. & Donahue, R. E. Exploring the variation of the $\delta^{18}O_p$ and $\delta^{18}O_c$ relationship in enamel increments. *Palaeogeogr. Palaeoclimatol. Palaeoecol.* **310**, 71–83, doi:10.1016/j.palaeo.2011.02.023 (2011).

157 Munro, L. E., Longstaffe, F. J. & White, C. D. Burning and boiling of modern deer bone: Effects on crystallinity and oxygen isotope composition of bioapatite phosphate. *Palaeogeogr. Palaeoclimatol. Palaeoecol.* **249**, 90–102, doi:http://dx.doi.org/10.1016/j.palaeo.2007.01.011 (2007).

158 Bar-Yosef, O. & Belmaker, M. in *Quaternary of the Levant: Environments, climate change, and humans* (eds Ofer Bar-Yosef & Yehouda Enzel) 179–186 (Cambridge University Press, 2017).
159 Heller, J. & Sivan, N. *Melanopsis* from the Pleistocene site of 'Ubeidiya, Jordan Valley: Direct evidence of early hybridization (Gastropoda: Cerithioidea). *Biol. J. Linn. Soc. Lond.* **75**, 39–57, doi:10.1046/j.1095-8312.2002.00005.x (2002).
160 Bar-Yosef, O. & Tchernov, E. *On the palaeo-ecological history of the site of 'Ubeidiya*. 1–35 (Israel Academy of Sciences and Humanities, 1972).
161 Dettmann, D. L. *et al.* Seasonal stable isotope evidence for a strong Asian monsoon throughout the past 10.7 m.y. *Geology* **29**, 31–34 (2001).
162 Tütken, T., Vennemann, T. W., Janz, H. & Heizmann, H. E. P. Palaeoenvironment and palaeoclimate of the Middle Miocene lake in the Steinheim basin, SW Germany, a reconstruction from C, O, and Sr isotopes of fossil remains. *Palaeogeogr. Palaeoclimatol. Palaeoecol.* **241**, 457–491 (2006).
163 Vennemann, T. V., Fricke, H. C., Blake, R. E., O'Neil, J. R. & Colman, A. Oxygen isotope analysis of phosphates: a comparison of techniques for analysis of Ag_3PO_4. *Chem. Geol.* **185**, 321–336, doi:https://doi.org/10.1016/S0009-2541(01)00413-2 (2002).
164 Spiro, B. *et al.* Climate variability in the Upper Jordan Valley around 0.78 Ma, inferences from time-series stable isotopes of Viviparidae, supported by mollusc and plant palaeoecology. *Palaeogeogr. Palaeoclimatol. Palaeoecol.* **282**, 32–44, doi:https://doi.org/10.1016/j.palaeo.2009.08.005 (2009).
165 Robinson, J. R. & Kingston, J. D. Burned by the fire: Isotopic effects of experimental combustion of faunal tooth enamel. *J. Archaeol. Sci.* **34**, 102593, doi:https://doi.org/10.1016/j.jasrep.2020.102593 (2020).
166 Stiner, M. C. *et al.* Bone preservation in Hayonim Cave (Israel): A macroscopic and mineralogical study. *J. Archaeol. Sci.* **28**, 643–659, doi:10.1006/jasc.2000.0634 (2001).